Journal of Solid State Electrochemistry (2023) 27:813–839
https://doi.org/10.1007/s10008-023-05387-z

REVIEW PAPER

Cathode materials for lithium-sulfur battery: a review

Ryohei Mori[1,2]

Received: 15 October 2022 / Revised: 20 December 2022 / Accepted: 7 January 2023 / Published online: 20 January 2023

Abstract
Lithium-sulfur batteries (LSBs) are considered to be one of the most promising candidates for becoming the post-lithium-ion battery technology, which would require a high level of energy density across a variety of applications. An increasing amount of research has been conducted on LSBs over the past decade to develop fundamental understanding, modelling, and application-based control. In this study, the advantages and disadvantages of LSB technology are discussed from a fundamental perspective. Then, the focus shifts to intermediate lithium polysulfide adsorption capacity and the challenges involved in improving LSBs by using alternative materials besides carbon for cathode construction. Attempted alternative materials include metal oxides, metal carbides, metal nitrides, MXenes, graphene, quantum dots, and metal organic frameworks. One critical issue is that polar material should be more favorable than non-polar carbonaceous materials in the aspect of intermediate lithium polysulfide species adsorption and suppress shuttle effect. It will be also presented that by preparing cathode with suitable materials and morphological structure, high-performance LSB can be obtained.

Keywords Lithium-sulfur battery · Lithium polysulfide · Shuttle effect · Cathode · Sulfur · Composite

Introduction

Various types of new energy storage technologies such as multi-ion batteries, sodium-ion batteries, metal-air batteries, ultra-capacitors, all-solid-state batteries, and redox-flow batteries are currently under development. The lithium-sulfur battery (LSB) is one of the most promising candidates to be the next-generation rechargeable battery, i.e., the post-lithium-ion battery [1–3]. When compared with the current forms of the lithium-ion battery (LIB), LSBs have higher specific energy (calculated to be approximately 6–7 times that of their LIB equivalent), superior safety, and lower unit cost due to the relatively high availability of sulfur [4–8]. As a result, there has been a significant amount of LSB research carried out over the past decade with a focus on developing fundamental understanding, modelling, and component materials. Although the LSB battery has not yet been commercialized because of its undesirable high self-discharge rate and short cycle life, a tremendous number of challenges have been overcome in order to remedy these faults by clarifying the fundamental scientific mechanisms behind LSB cell behavior and component materials [9, 10]. In the following sections, we will begin with a discussion of the advantages of the LSB as well as its limitations, followed by a discussion of the development of materials and mechanisms designed to alleviate the current limitations of the battery.

LSB technology: advantages and limitations

The LSB is an electrochemical cell with a high gravimetric energy potential. Its theoretical specific capacity is 1675 $mAhg^{-1}$ (2500 Wh kg^{-1}), a result of the 16-electron reduction of an S_8 molecule at the cathode:

$$S_8 + 16e^- + 16Li^+ \rightarrow 8Li_2S \quad (1)$$

The working mechanism underlying LSB functionality is highly complicated and is, in fact, still the subject of debate although the main principle can be summarized as follows. In general, the primary LSB components are the lithium-metal anode, the sulfur-containing cathode, a carbon-based material, and a binder. There is also a separator and an electrolyte between the anode and cathode [11].

✉ Ryohei Mori
moriryohei@fuji-pigment.co.jp; ryoheimori@gsalliance.co.jp

[1] Green Science Alliance Co., Ltd., 2-22-11 Obana, Hyogo Prefecture, 666-0015 Kawanishi City, Japan

[2] Fuji Pigment Co., Ltd., 2-23-2 Obana, Hyogo Prefecture, 666-0015 Kawanishi City, Japan

During discharge, the sulfur in the cathode dissolves into the electrolyte, forming S8. The liquid S8 is then electrochemically reduced at the cathode to form several intermediate products, referred to as lithium polysulfide (LiPS) species (Li_2S_x), with an accompanying oxidation of Li metal into Li + ions at the anode. From the cathode side, the polysulfide species (Li_2S_x, $2 < x \leq 8$) diffuse to the electrolyte/separator side because they are soluble in the electrolyte liquid. As discharge reaction proceeds, the length of the polysulfide chains reduce, which affects the liquid electrolyte viscosity, mobility, and solubility of the Li_2S_x compounds.

After discharge is complete, the S_8 is fully reduced to S_2^- (Li_2S) and the anode is fully stripped of Li metal. The reverse reactions occur during the charging stage. Li^+ ions deposit at the anode as the Li metal and low-order polysulfides oxidize from S_2^- up to S_{2-8} and eventually become S_8. This process is illustrated in Fig. 1 [12–14].

Advantages of a lithium-sulfur system

Sulfur, the raw material of the LSB cathode, is cheap, abundant, and non-toxic; therefore, the LSB is a more environmentally and economically friendly option than the heavy transition metal–based LIB. The cell cost of an LSB can also be lower than that of an LIB (approximately 100 USD per KWh) [4, 15, 143]. Another of its advantages is that an LSB can be discharged to a 0% charge state and does not need to be subsequently recharged for storage [144, 145]. This means that an LSB can be left in a discharged state for long-term storage periods when it is not in use without serious capacity degradation. This is rather significant, as LIBs need to be recharged before long-term storage in order to prevent irreversible capacity loss. Furthermore, its component materials allow for a very light weight, as little as 1 gcm^{-3}, which is much lighter than a typical LIB. This is another significant edge that LSBs have over LIBs, because aeronautical and submarine applications require rechargeable batteries to be as light as possible [16, 146, 147].

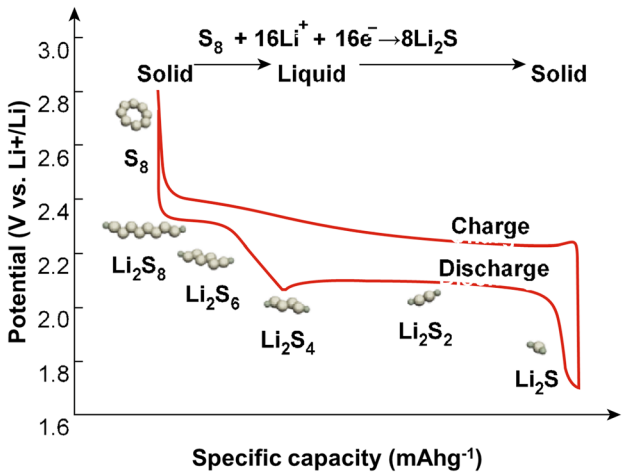

Fig. 1 A typical charge/discharge profile for LSB

Limitations of lithium-sulfur batteries

Despite its extremely high theoretical energy density, the LSB has a significantly lower practical energy density value, which is one of the key obstacles to the commercialization of LSBs. The complex working mechanism of the LSB is one of the reasons behind this. Specifically, the problem lies in the conversion of elemental sulfur (S_8) into the final reduction product, lithium-sulfide (Li_2S). A non-trivial amount of effort has been exerted to overcome this obstacle. During the discharge process, elemental sulfur is reduced into a soluble form of an intermediary, LiPS (Li_2S_x, $3 < x < 8$), which is soluble in the electrolyte and can then diffuse out from the cathode.

As the discharge process continues, the length of the soluble polysulfide chains reduce, affecting electrolyte viscosity. Li_2S_2 and Li_2S are the final discharge products, solid insulating substances that can enhance LSB resistance by passivating the conductive surface of the cathode. The charge process is also quite complicated, involving solid products (Li_2S_2/Li_2S) oxidizing back into the soluble form and ultimately converting into elemental sulfur. This last step depends on the charge cut of the voltage [17].

It is not possible to clearly distinguish individual polysulfide species and the reaction varies greatly depending on the electrolyte/electrode combination. The physical and chemical properties, as well as the structure of the electrode and electrolyte (polysulfide affinity, reactivity to lithium metal, dielectric constant, viscosity, molecular structure of electrode, etc.), can critically affect the rate of each of the reaction steps inside an LSB [14, 18, 19]. For instance, a dense cathode may have a large surface area such that a high capacity would be expected, although a low-viscosity electrolyte would be necessary in that case; otherwise, the electrolyte would not be able to penetrate through the entire thickness of the cathode film, thereby suppressing the efficient mass transport of species in the solution. This tendency is more severe in the case of an LSB compared to an LIB since the shuttling of Li^+ ions between the anode and the cathode is the major reaction for the latter one. Even this example is sufficient to make matters difficult for researchers, complicating the decision as to which material they should choose to make an LSB. The potential incompatibilities between high-performance component materials also imply that experiments need to be performed individually and in an isolated environment for each material.

The use of lithium metal for the anode can also suffer from its own limitations, despite its high theoretical and gravimetric energy capacity. The short cycle life of an LSB

is primarily attributable to the use of lithium metal. Lithium is a highly electronegative element with a reduction potential of − 3.04 V. Because of this high potential, almost all organic solvents will spontaneously react with it, resulting in severe electrolyte degradation [20]. Furthermore, polysulfide formed at the anode surface reduces to a shorter polysulfide, lowering the coulomb efficiency and causing irreversible loss of the active material from the cathode.

The stripping and plating of lithium ions during charge and discharge gives rise to an uneven lithium metal anode surface as the reaction proceeds. This causes an inhomogeneous current density distribution across the LSB. This is of concern because an excessive proportion of uneven surface could impact the other cell components, most notably the cathode, leading to a short circuit [21–23].

Alternative materials such as graphite and silicon (Si)– and tin (Sn)–based materials have been tried as substitutes for lithium metal in LSB anodes [24–26]. It should be noted that these materials need to be lithiated in order to function as anode for LSB. However, the resulting anodes are less electronegative than Li, further reducing the battery potential; at ~ 2.1 V, this is already lower than Li-ion batteries. Si or Sn is also more than an order of magnitude heavier than lithium metal, one of the lightest elements; therefore, the total weight of the Si or Sn-based negative electrode increases, negatively impacting the specific energy and gravimetric energy density of the final cell. In addition, the volume of a Si or Sn-based anode changes dramatically during the charge–discharge cycle, ultimately deteriorating the LSB itself [27]. In light of this, lithium metal still appears to be the best anode material that actualizes the full potential of the Li–S multi-electron reduction.

The battery cycle life is also deteriorated by the deposition of poorly soluble/insoluble products (i.e., Li_2S_2 and Li_2S) at the cathode, formed due to the decomposition of the cathode carbon skeleton and polysulfide reaction with the electrolyte [28]. Sulfur is an active material in an LSB, although its intrinsic nature as an insulator necessitates a large amount of conductive carbon material to keep the cathode conductive. Thus, in general, LSBs require a much larger quantity of conductive carbon material to be introduced into their cathodes compared to LIBs, creating porous structures that can collapse under the repetitive charge–discharge cycles of deposition and dissolution of active materials, which are in the form of different lengths of LiPS. Researchers have been trying to solve this issue by modifying the cathode to allow for rapid mass transfer and redox reactions [29, 30]. A low-density electrolyte also facilitates rapid Li^+ diffusion. A sulfur cathode experiences large-volume change during charge–discharge cycles, which is also the main reason for the gradual destruction of the electrode because of eventual delamination from the current collector. In short, intermediate LiPS is the main cause of LSB deterioration.

Looking more closely into cathode materials, the carbon or carbonaceous materials used as the conductive material generally exhibit a non-polar surface. Non-polar surfaces usually have only weak interactions with highly polar LiPS, resulting in the dissolution of LiPS and severe capacity fade [31–33]. Thus, to suppress LiPS shuttle and improve cell cycle life, a cathode material that possesses a polar surface, such as an oxide, a nitride, or a carbide, would be more ideal for the suppression of LiPS dissolution through chemisorption and chemical anchoring.

It should be noted here that some carbonaceous materials can possess polar surface by nitrogen, sulfur, phosphor doping, or some transition metal doping such as cobalt, nickel, and iron. Additionally, different type of carbonaceous materials such as carbon nanotube, and graphene also should also show some non-polar surface depends on their morphology and surface edge [155–161].

Despite all these difficulties, however, the LSB is still the most promising candidate for the next-generation rechargeable battery, largely owing to its high theoretical capacity.

In the following section, various types of cathode material will be discussed in order to improve the electrochemical properties of LSB, classified by its material component.

Cathode materials

Sulfur-metal oxide composite

Certain metal oxides exhibit electrocatalytic activity toward LiPS adsorption, and the strong interaction between a polar surface and LiPS during the electrochemical reaction is an important factor for this adsorption. MnO_2 [34], WO_{3-x} [35], V_2O_5 [36], $LaMnO_{3-\delta}$ [37], CeO_2 [38], SnO_2 [39], ZrO_2 [40], TiO_2 [41], and other composites have all been applied to trap LiPS and improve LSB electrochemical reactions. Compared with pure sulfur, the S-TiO_2 composite showed a better discharge capacity retention of 58% after 50 cycles and a discharge capacity of 530 $mAhg^{-1}$ after 50 cycles, which can be ascribed to the adsorption of LiPS by TiO_2 [41].

An oxygen-deficient modified metal oxide–based cathode generally shows enhanced electrocatalytic activity in various types of electrochemical reaction. Oxygen-deficient WO_3 was used as an electrode for LSBs. The sulfur and oxygen-deficient WO_3 composite cathode showed a capacity decay of only 0.13% per cycle at a 0.5 C rate owing to the suppression of LiPS accumulation on the cathode surface from the interaction of the WO_3 and LiPS [35]. A CeO_2 and nitrogen-doped carbon composite material successfully mitigated LiPS dissolution and promoted rapid LiPS conversion reactions. The strong electrocatalytic effect also enhanced the LiPS redox reaction, which was confirmed by the positive and negative shifts in the reduction and

oxidation peaks of CV, respectively. The CeO_2-modified electrode exhibited a reversible capacity of 1064 mAh g^{-1} at a 0.2 C rate after 200 cycles [38]. Furthermore, owing to the strong interaction between the Fe_2O_3 nanoparticles and graphene, their combination proved to be an effective way to suppress LiPS shuttle. The conversion of soluble LiPS into insoluble Li_2S_2 and Li_2S was also accelerated. The adsorption energy of Fe_2O_3 toward LiPS, S_8, and Li_2S was revealed to be higher than graphene through DFT calculations. As a result, the sulfur-Fe_2O_3 composite electrode demonstrated a high capacity of 565 $mAhg^{-1}$ with a low-capacity decay of 0.049% per cycle for 1000 continuous charge–discharge cycles at a 5 C rate [42]. Other types of oxide material such as a Magnéli phase Ti_4O_7 was also investigated, confirming the enhancement of the LiPS redox chemistry. Ti_4O_7 magnéli phase is reported to behave as metallic due to delocalization of 3*d* electrons [132]. Pang et al. studied that sulfur host material that possess inherent metallic conductivity can have ability to chemically bind LiPS on the surface and facilitate reduction to Li_2S. A high surface area Magneli phase (Ti_4O_7) fulfills these requirements and demonstrates excellent cycle performance and high-rate capability. In addition, they have shown that polar O-Ti–O units in Ti_4O_7 have a high affinity for LiPS [43]. This concept is shown in Fig. 2. On a typical carbon support which is generally used as sulfur support material for LSB cathode, elemental sulfur experiences reduction to form LiPS then after dissolves into the electrolyte (Fig. 2a). Initial reduction offers S_8^{2-} that disproportionates in solution to elemental sulfur and S_6^{2-}. The soluble S_6^{2-} can either split to form soluble, reducible S_3^-; or further reduce to S_4^{2-} and ultimately precipitate Li_2S; and/or reduce and disproportionate to form a higher order LiPS and Li_2S. In any case, these solution-mediated reactions are highly complex and high concentration of LiPS accumulates that results in deposition of Li_2S with high interfacial impedance. In contrast, S_8 reduction on the metallic polar Ti_4O_7, LiPS adsorbs on the surface and is reduced to Li_2S via surface-mediated reduction and in this case, interfacial impedance can stay low which is more favorable for LSB electrochemical performance. Based on these facts, the

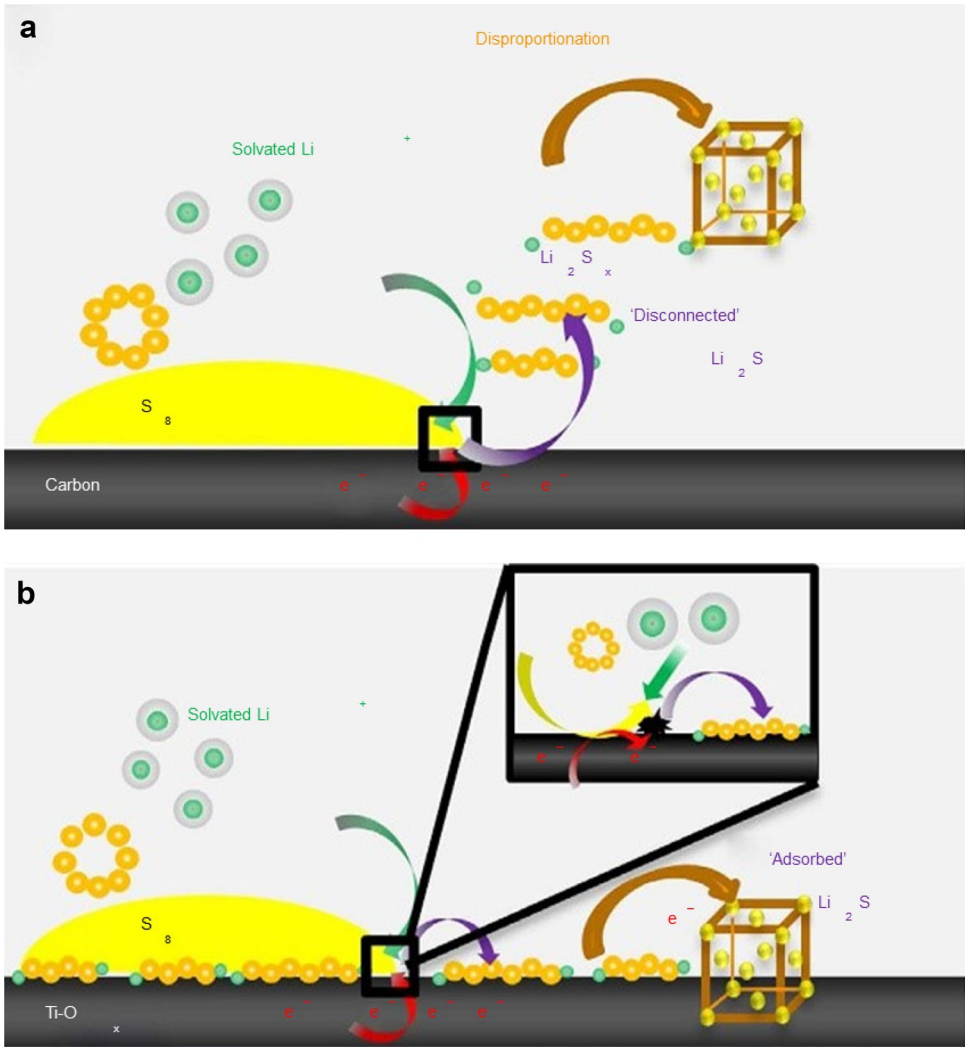

Fig. 2 Diagram illustrating surface-mediated reduction of Li_2S from LiPSs on Ti_4O_7. **a** On reduction of S_8 on a carbon host, LiPSs (Li_2SX) desorb from the surface and undergo solution-mediated reactions leading to broadly distributed precipitation of Li_2S. **b** On reduction of S_8 on the metallic polar Ti_4O_7, LiPSs adsorb on the surface and are reduced to Li_2S via surface-mediated reduction at the interface

Ti_4O_7-S composite cathode exhibited a discharge capacity of 1070 mAh g^{-1} at a moderate rate and delivered a stable cycle life of 500 cycles at a 2 C rate. It was suggested that when the sulfur/sulfide host is both sulfiphilic and metallic, redox is further facilitated [43, 132].

Besides particular oxides such as magnéli oxide material, perovskite, and cation vacancy oxide based on some transition metal such as copper, niobium, calcium, and vanadium, oxide have been studied to possess storage capacity against lithium, sodium, etc. [148–155].

Sulfur-metal sulfide composites

Metal-based chalcogenide electrocatalysts are considered a potential LSB cathode material owing to their relatively cheap cost, as well as their high performance and chemical stability against sulfur-based materials. Moreover, they avoid overlap with the active-voltage region in an LSB because of their low lithiation potentials [33].

Sulfide-based electrocatalytic materials can be generally metallic or semi-metallic, which promotes electron transfer during LiPS conversion reactions. The main reason for their superior electrocatalytic properties is their effective d-band structure, a product of the synergism between metal d-orbital and unsaturated S-heteroatoms. This results in similar properties to those determined by the d-band of Pt. Thus, the catalytic activity of the metal sulfide materials is correlated with the number of exposed edge sites [44]. Jaramillo also reported that electrocatalytic activity for hydrogen evolution correlates linearly with the number of edge sites on the MoS_2 catalyst for example [133]. Karunadasa et al. also prepared a molecular modelling one of these edge sites, in which a triangular Mo-S–S unit was supported by metal coordination to five tethered pyridine rings, and demonstrated that these edge sites were active toward electrochemical generation of hydrogen from water. They had also suggested that this type of materials can be a low-cost alternative to platinum for electrocatalytic hydrogen production [134]. Wu et al. had reported that the catalytic properties of monometals and binary alloys can be realized in terms of the electronic structures of the principal elements both experimentally and theoretically (i.e., d-band theory) [135]. For example, deposition of platinum on the gold nanoparticle catalyst modulates its d-band electronic structures, with the electronic energy tunable between − 3.93 and − 4.24, approximating that of chemically resistant gold (− 4.35 eV). This reaction will weaken the binding strength between Pt active sites and intermediate species which resulted in obtaining higher catalytic activity [136].

Thus far, a number of sulfide-based catalysts have been investigated with a focus on LiPS conversion reactions, including WS_2, MoS_2, SnS_2, CoS_2, and binary sulfides [45]. Zhang et al. used CoS_2 as an electrocatalyst in an LSB in an attempt to achieve efficient LiPS conversion. CoS_2 is semi-metallic and has a conductivity of 6.7×10^3 Scm^{-1} at 300 K, which is relatively high compared to first-row transition metal sulfides such as Ni_3S_2 and FeS_2. Due to the sulfiphilic nature and high electron conduction of CoS_2, the LiPS redox reactions were indeed accelerated [46]. It was found that the WS_2 enhanced the charge transfer kinetics in the LSB due to the catalytic active edge sites of WS_2. The interaction between LiPS and WS_2 edge sites was investigated with scanning electron microscopy (SEM), XPS, and UV–Vis spectroscopy. The results demonstrated that the unsaturated edge atoms of the transition metal dichalcogenide experienced significant LiPS adsorption due to the polarity and inherent catalytic activity. As a result, a specific capacity of 590 mAh g^{-1} and catalytically driven stable Coulombic efficiency of 99% for 350 continuous charge–discharge cycles were obtained [47].

MoS_2 and its oxygen-deficient form, as well as their graphene oxide composite, were tested as electrodes for an LSB [9]. Cyclic voltammetry (CV) was measured to understand the catalytic effect of MoS_{2-x} on the LiPS redox reactions. As presented in Fig. 3, the catalytic effect of MoS_{2-x} on the polysulfide redox reactions was investigated by CV in symmetric cells with identical working and counter electrodes in a 0.2 M Li_2S_6 electrolyte. MoS_2/rGO and rGO prepared under the same conditions were used as the experimental controls. To clarify capacitive contribution, the CV of a Li_2S_6-free electrolyte was also analyzed for correction. The CV of the MoS_{2-x}/rGO electrode in the Li_2S_6 electrolyte clearly indicated high reversibility with four distinct peaks at − 0.047 V, − 0.39 V, 0.047 V, and 0.39 V respectively (Fig. 3A). On the other hand, the MoS_2/rGO electrode showed these peaks as broad redox features at − 0.31 V, − 0.61 V, 0.31 V, and 0.61 V (Fig. 3B). For the rGO electrode, only a very drawn-out reduction peak at − 1.22 V and a another drawn-out oxidation peak at 1.22 V were observed (Fig. 3C). At these measurements, only Li_2S_6 was the electrochemically active species in the electrolyte so that one can deduce that Li_2S_6 was reduced to Li_2S (or Li_2S_2) on the working electrode, and oxidized to sulfur on the counter electrode. The narrow peak separation and distinctive individual peaks clearly prove that stable electrochemical reversibility and facile polysulfide conversion is possible only for oxygen-deficient form MoS_2 [9].

Cho et al. also experimented with nitrogen-doped MoS_2 as an LSB cathode. The nitrogen-doped MoS_2 increased the chemisorption energy of LiPS and promoted electron transfer, resulting in improved cycle stability and electrochemical properties. In addition, it amplified the redox kinetics of the LiPS by acting as a catalyst for the cathode. The nitrogen-doped MoS_2 accelerated the reaction rates by reducing the activation energy barrier of Li_2S_n to Li_2S conversion and inhibited the shuttle effect by rapidly reducing

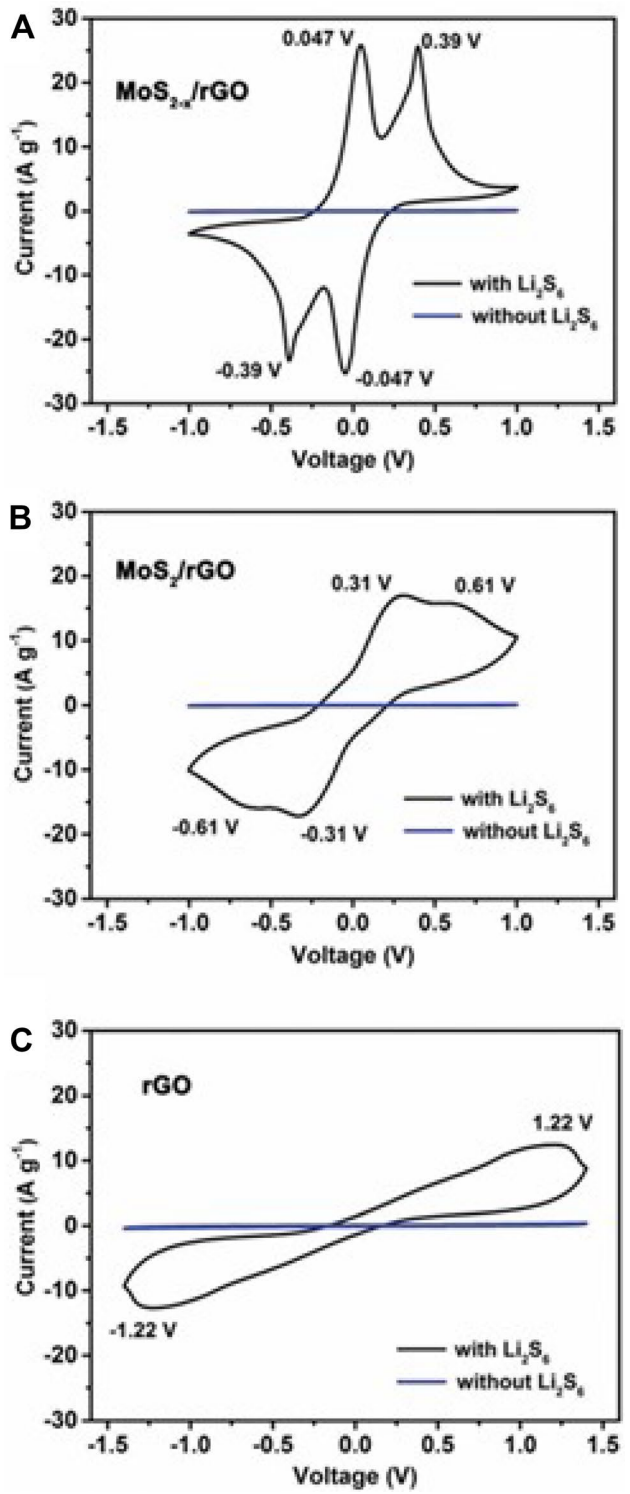

Fig. 3 Cyclic voltammograms of symmetric cells with identical electrodes of (**A**) MoS_{2-x}/rGO, (**B**) MoS_2/rGO, and (**C**) rGO in electrolytes with and without 0.2 M Li_2S_6 at 3 mV/s

the highly soluble Li_2S_n. Ultimately, a high cycle stability with a low-capacity decay rate of 0.025% per cycle after 1000 cycles was observed [48].

Sulfur-metal carbide composites

Transition metal carbide–based hydrophilic materials are another strong candidate material that can bind to LiPS and enhance LSB redox reactions. The intrinsic electrochemical activity of transition metal carbide originates from the number of electrons in the 3d subshell of their atoms and the strong interactions between the metals and the electroactive species. It should be mentioned that the surface reactivity of transition metal carbide can behave in a similar manner to noble metals under certain conditions [49–51]. In addition, metal carbides inherently possess large interlayer channels that are known to shorten the ionic/electronic transport pathways, which could improve electrochemical properties. For example, tungsten carbide (WC)– and titanium carbide (TiC)–based cathodes were prepared and evaluated for use in an LSB. Spin-polarized DFT calculations were performed to examine the details of the adsorption state of Li_2S_8 on metal carbide. It was found that Li_2S_8 dissolved on the metal carbide upon adsorption, whereas it did not dissolve on the carbonaceous materials. WC and TiC exhibited higher binding energies with Li_2S_8 compared to graphene because of the polar metal carbon bonds of the former and the non-polar carbon–carbon bonds of the latter.

Binding energies against Li_2S_8 was 3.56 eV/S atom and 3.68 eV/S atom for WC and TiC, respectively. It was 0.11 eV/S atom for graphene which clearly demonstrates that different way of chemical bonding toward Li_2S_8 critically influences the binding energy.

UV–Vis spectroscopy confirmed that the adsorption strength of W and Ti edge sites with LiPS was high. Owing to these advantages, the battery capacity was 1156 $mAhg^{-1}$, and excellent reversibility was confirmed when TiC was used as the electrode material [52]. The role of conductive polar TiC on LiPS against Li_2S precipitation was further confirmed by comparing the results with those of a non-polar carbon and TiO_2 surface via first principles calculation. The binding energies between the TiC surface and Li_2S_4 and Li_2S were – 1.89 eV and – 2.75 eV, respectively, much greater than that with non-polar carbon. This confirmed that the high conductivity of TiC was effective for transforming LiPS [53].

Choi et al. investigated the properties of a WC-based cathode founding that it not only offers strong sulfiphilic surface moieties but also provides an efficient catalysis to promote polysulfide fragmentation, thereby drastically improving the electrode kinetics. WC can be a superb anchoring material for long-chain polysulfide and promote the dissociation of short-chain polysulfide. The effectiveness of WC on promoting the dissociation of short-chain polysulfides more clearly, they designed a chronoamperometric experiment for the solution containing Li_2S_4 polysulfides using the glassy carbon and polycrystalline WC electrodes. UV–vis spectroscopy was measured to visualize the change of S_4^{2-} species concentration

by the chemical disproportionation. Measurement indicates that WC has a significant influence on accelerating the Li_2S_4 disproportionation of (Fig. 4a, b), as the absorption peak centered at 410 nm (which is associated with Li_2S_4) for the WC electrode decreases much faster along with reaction time than the glass carbon electrode. This phenomenon was also visually proved in Fig. 4c and d, where much thinner color was observed for the solution treated with the WC electrode. As a result, LSB delivered an enhanced discharge capacity of 780 mA h $g.^{-1}$ at a current rate of 0.5 C (Fig. 5) [54].

In addition, boron carbide nanowires were investigated as an LSB cathode material. The surface of boron carbide was revealed to be an effective trap for LiPS, and DFT calculations further revealed that the boron carbide had a high binding energy (3.84–12.51 eV) with Li_2S_4 compared with the non-polar graphite surface (1.18 eV). Bader charge analysis elucidated that the electron density increased between sulfur and boron carbide, which was the main cause for chemical bond formation between Li_2S_4 and boron carbide. The results also indicated that the intrinsic catalytic property of boron carbide could lower the over potentials as well as promote LiPS conversion. A boron carbide–based electrode could eliminate the need for an additional current collector or binder, thereby enabling the utilization of more sulfur content. The boron carbide nanowire–based electrode exhibited an initial capacity of 1024 $mAhg^{-1}$, which reduced to 815 $mAhg^{-1}$ after 500 cycles [55].

Sulfur-metal nitride composites

Carbon is a good host material for sulfur, and cathodes made of a composite of the two materials have been applied in the past. However, low tap densities of this composite often result in low volumetric energy density because it allows only a small amount of sulfur to be loaded. In this regard, a conductive porous vanadium nitride/sulfur composite without any carbonaceous material was used as the cathode material for an LSB. It obtained a reversible capacity of 790 mAh g^{-1} at 1 C after 200 cycles and 145.2 mAh g^{-1} at 15 C after 500 cycles. The use of porous laminated vanadium nitride as a sulfur host provides both the merits of a multiscale stacking structure and the attractive intrinsic properties of vanadium nitride. As an effective sulfur host, the porous laminated stacking network provides more space for sulfur storage, improves the tap density of the cathode, and promotes the rapid transfer and diffusion of lithium ions. The strong chemical anchoring of polar vanadium nitride with polysulfide also effectively inhibits exorbitant dissolution of LiPS. In addition, the excellent conductivity and catalytic activity of vanadium nitride enhance the conversion of

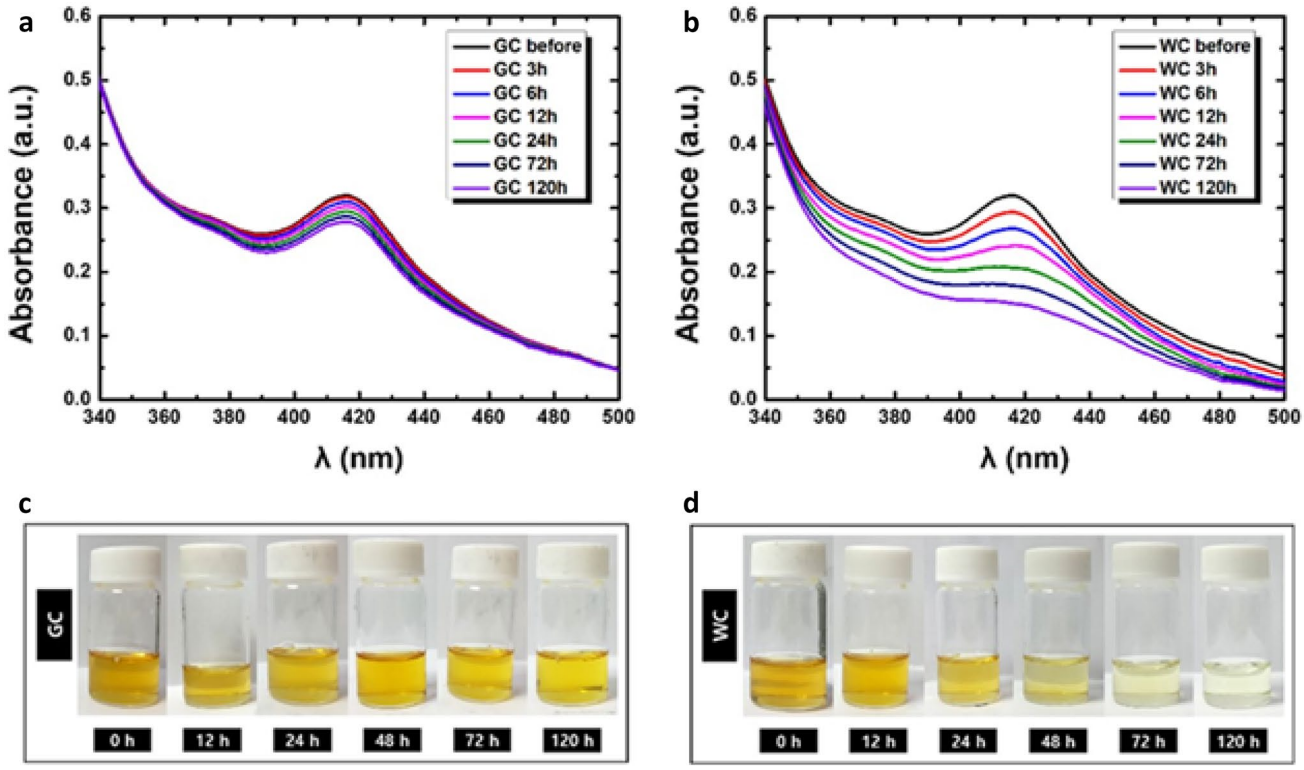

Fig. 4 UV–vis spectra measured with (**a**) carbon and (**b**) WC in the electrolyte containing 50 mM Li_2S_4; photographs of the electrolyte with (**c**) carbon and (**d**) WC

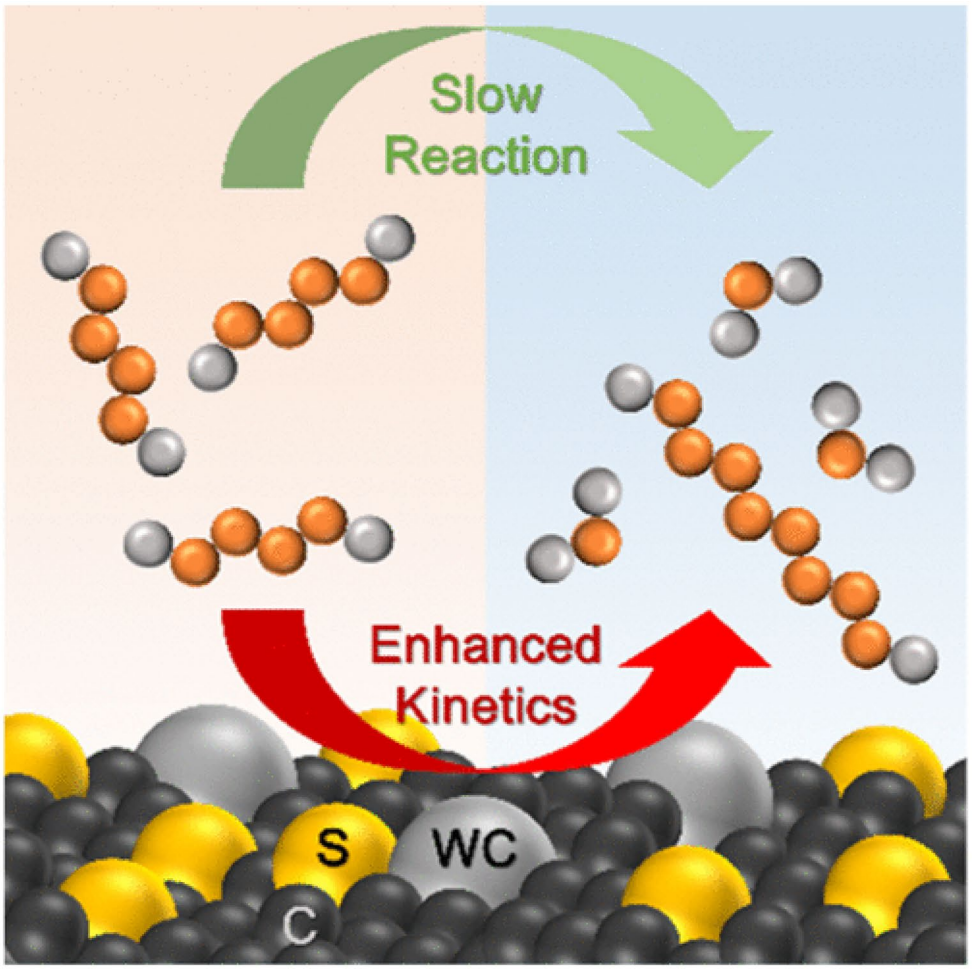

(a)

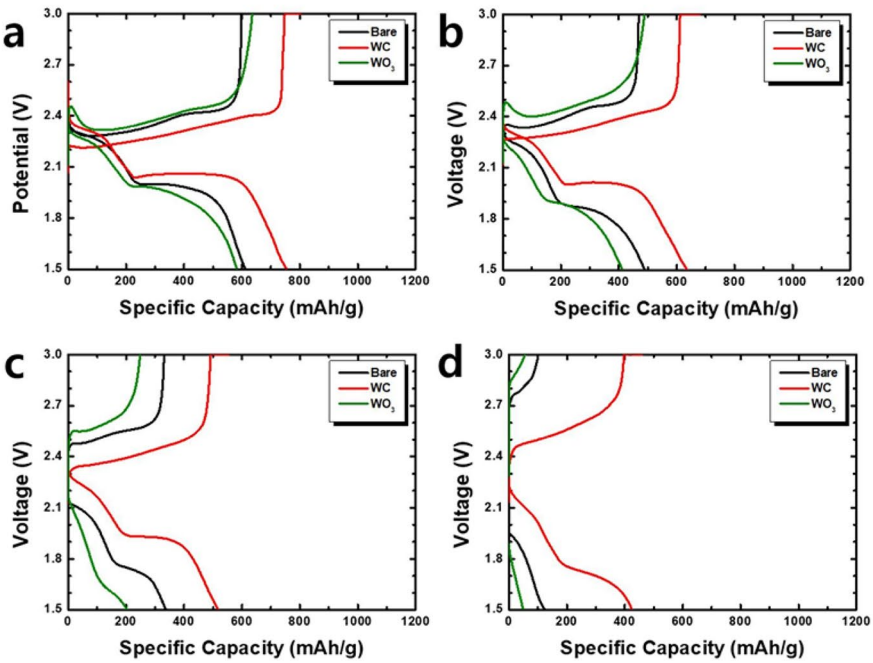

(b)

Fig. 5 **a** Schematic image of electrochemical reaction of lithium polysulfide on sulfide on tungsten carbide composite cathode material. **b** Charge–discharge profiles of the bare, WC, WO_3-loaded cell at (**a**) 0.5 C, (**b**) 1 C, (**c**) 2 C, and (**d**) 5 C

Li_2S to soluble LiPS, improving the redox reaction kinetics. Overall, the vanadium nitride cathode exhibited excellent LSB cycling performance (Fig. 6) [56].

Carbon nitride was also used as the cathode material in an LSB. A silica-template nano-casting method was used to synthesize mesoporous carbon nitride–based materials. The capacities of 1284.5 and 1107.1 mA h g^{-1} at 0.1 and 0.5 C, respectively, were initially observed. After 100 cycles, 1107.1 mA h g^{-1} was confirmed at 0.5 C. These high performances are due to the crosslinked mesoporous structure and the strong chemical interactions between sulfur and the carbon- and nitrogen-based material framework, which provided polysulfide reservoirs and transport channels for the transportation of ions and electrons. They were also effective in restraining polysulfide migration [57].

A TiN-S composite cathode demonstrated excellent electrochemical properties due to its relatively high electrical conductivity and strong N-S surface bonding. It also possessed a strong ability to capture soluble intermediate species [58]. Another TiN study demonstrated the preparation of nanostructured titanium nitride (TiN) and graphene composite electrodes by combining ultrasonication with the melt-diffusion of elemental sulfur. TiN nanoparticles and tube arrays were mechanically mixed with the graphene substrate and a porous composite structure with enhanced electrical conductivity was formed. Such a cathode promoted the accessibility of the electrolyte and the rapid transfer of charges, resulting in 1229 and 1085 mAh g^{-1}, respectively, at 1 st cycle and after 180 cycles under a 0.1 C rate [59].

Conductive hollow cobalt nitride–carbon ($Co_{5.47}N_x$-C) spheres with nitrogen vacancies were used as a cathode material. Dopamine was coated on porous silica template and carbonized under argon flow at 800 °C. To obtain hollow carbon spheres, aqueous HF solution etching was

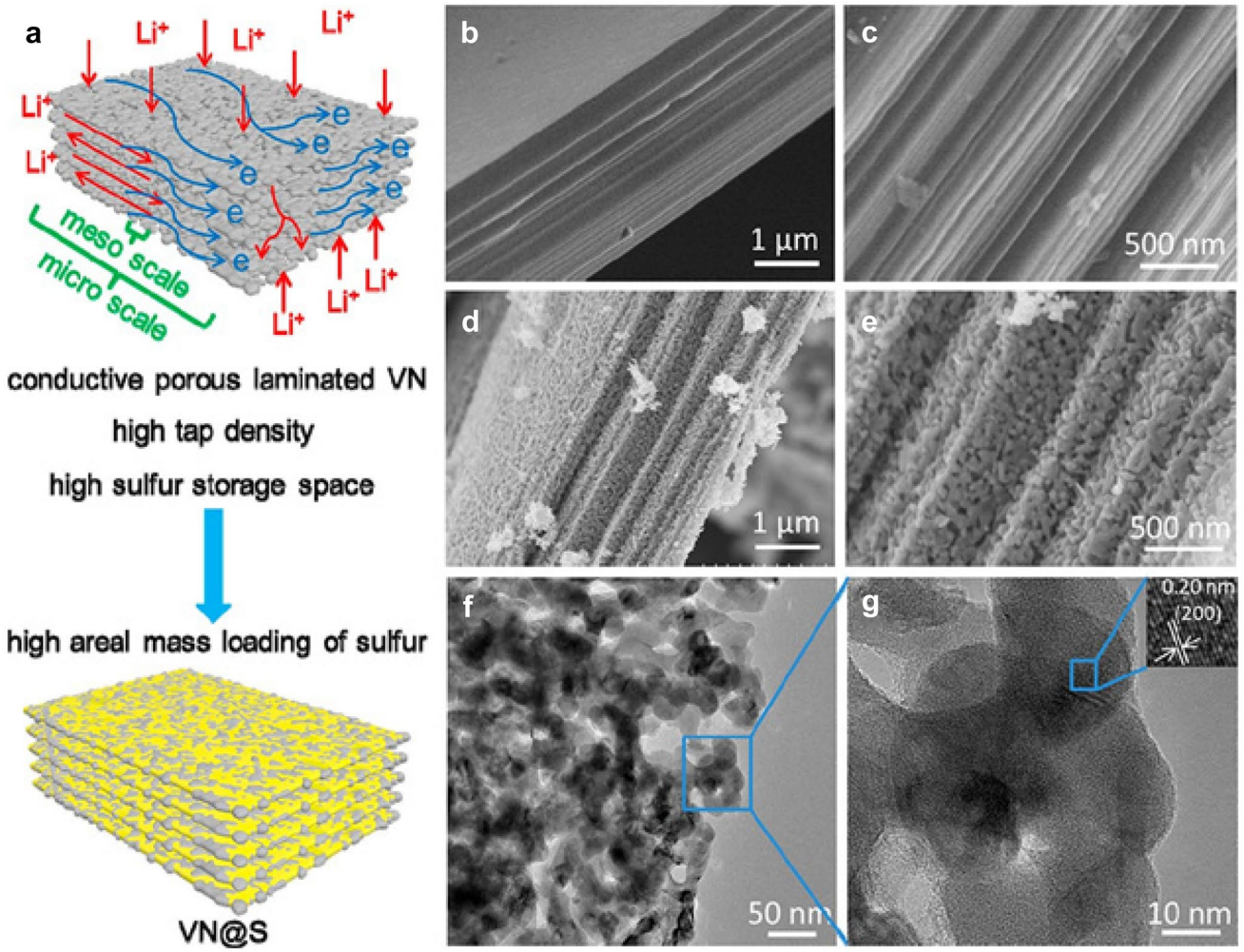

Fig. 6 **a** Schematic of the conductive porous laminated VN and VN / S's internal structure. **b**, **c** Different magnification SEM images of laminated V_2O_5 microsheets. **d**, **e** Different magnification SEM images of porous laminated VN microsheets. **f**, **g** Different magnification TEM images of porous laminated VN microsheets. **g** (inset) HRTEM image of VN nanoparticles [56]

performed to remove silica. Acidification of hollow carbon spheres were achieved by refluxing with HNO_3 and H_2SO_4 mixture at 70 ℃. Then, this acidified hollow carbon was added to $CoCl_3$ and 2-methylimidazole solution to synthesize ZIF-67 together, then annealed in ammonia at 600℃ to obtain final hollow $Co_{5.47}N_x$-C spheres. Due to its Co–N bonds and nitrogen-vacancy sites, the $Co_{5.47}N_x$-C composite can achieve strong anchoring of the polysulfides, fast polysulfide conversion, and accelerated lithium-ion transport. The strong anchoring effect of the $Co_{5.47}N_x$ was confirmed experimentally and by DFT calculations. Its high conductivity and nitrogen vacancies of the $Co_{5.47}N_x$ cathode improved the effectiveness of the redox reaction kinetics and lowered the polarization compared with a $Co_{5.47}N_x$ cathode, showing excellent rate and cycling performance, with a capacity of 850 mA h g^{-1} at 0.5 C and a rate performance of 320 mA h g^{-1} at 10 C [60].

Sulfur-MXene composites

Since the discovery of graphene and its excellent properties, two-dimensional (2D) materials became the focus of an aggressive research program in materials science [61–63]. Recently, a new family of 2D materials has emerged, which consists of transition metal carbides, nitrides, and carbonitrides; these are collectively known as MXenes [64, 65]. These novel materials can be prepared by selectively etching layers of sp elements from their corresponding three-dimensional (3D) MAX phases. These MAX phases are layered ternary metal carbides, nitrides, or carbonitrides, with the general formula of $M_{n+1}AX_n$ ($n = 1, 2, 3$), where M, A, and X represent early d-block transition metals, main-group sp elements (predominantly IIIA or IVA), and either or both C and N atoms, respectively. Thus far, more than 70 MAX phases have been presented [66]. The major forms of MXene are Ti_3C_2 [67], Ti_2C [68], $(Ti_{0.5}, Nb_{0.5})_2C$, $(V_{0.5}, Cr_{0.5})_3C_2$, Ti_3CN [69], Ta_4C_3, Nb_2C, V_2C, and Nb_4C_3, and some additional MXene materials are expected to be developed in the future. One interesting feature of this material is that the outer surfaces of the exfoliated layers always terminate with F, OH, and/or O groups during the etching process. Thus, these terminated MXene species are referred to as $M_{n+1}X_nT_x$, where T represents the surface groups (F, OH, and/or O) and "x" is the number of terminations. MXenes have been reported to possess exceptional properties. For example, the conductivity of MXenes is comparable to that of multilayered graphene [70]. They are also considerably stiff, with in-plane elastic constants exceeding 500 GPa [71].

These fascinating properties could lead to important applications and have attracted much attention from researchers in multiple fields. In the field of energy storage specifically, MXenes are considered to be strong candidates as materials for electrodes [72, 73]. MXenes are also an extremely interesting and potential material for LSB cathodes because of their inherent high conductivity and highly active 2D surface that can chemically bond with intermediate LiPS via metal-sulfur interaction.

MXene phase Ti_2C was shown to be an effective sulfur host material for LSBs. This type of material has high 2D electron conductivity and exposed terminal metal sites that can bind LiPS. It was clarified that the Ti–OH groups in MXene Ti_2C nanosheets are replaced by Ti-S at elevated temperatures during sulfur infusion. One study found that the electronegative S atoms decreased the electron density of Ti atoms, resulting in a higher binding energy for the Ti-S bond compared with that for the Ti-C bond. Therefore, the anchoring of LiPS to the Ti_2C surface was higher because of the Lewis acid–base interactions between Ti and S. The composite material demonstrated excellent cycling performance with a specific capacity of approximately 1200 mA h g^{-1} at a 5-h charge–discharge (C/5) current rate. A capacity retention of 80% was achieved over 400 cycles at a 2-h charge–discharge (C/2) current rate [74].

The surface terminations of MXene are a critical factor in the adsorption of LiPS. The type and number of functional groups and their specific mechanisms to suppress shuttling of LiPS are the key issue. Rao et al. investigated the effect of the interaction between Ti_2C without surface terminations and LiPS [75]. The DFT calculations clarified that a strong Ti-S bond formed by the S elements in LiPS and the Ti element in Ti_2C was a major obstacle to reversible reaction. The introduction of terminations Ti_2CF_2, $Ti_2C(OH)_2$, and Ti_2CO_2 improved the LSB properties by weakening the Ti-S bond. Thus, it is critical to examine MXene surface terminations. Ti_2CO_2 and $Ti_3C_2O_2$ MXenes with -O terminations exhibit a dual adsorption mechanism in LSBs, namely Li–O adsorption and Ti-S adsorption. The negatively charged O atoms combine with the positively charged Li + in LiPS, which results in a binding energy of 1–2 eV [76]. Additionally, the presence of Li–O bonds weakens the Li–S interactions in higher order LiPS, converting it to lower orders and accelerating the reaction process.

The anchoring behavior of O/F-functionalized Ti_2C MXene on LiPS was also investigated through DFT calculations by Sim and Chun [77]. They suggested that neither a single O-functionalized surface nor a single F-functionalized surface were as strong in LiPS adsorption as multiple functional group-functionalized MXene. The elimination of surface functional group vacancies had a more dramatic effect. Moreover, Ti_2CS_2 MXene with S terminations showed a stronger anchoring ability to LiPS than O/F-surface-terminated MXene (Fig. 7a).

Theoretical calculations of single-layer Ti_2C and Ti_2CS_2 without adsorbed LiPS showed that Ti_2CS_2 retains its metallic properties, therefore enhancing its electrochemical properties [78]. Titanium nitride MXene (Ti_2N) is also regarded as

a promising cathode host material for LSBs. Lin studied the interaction of O-functionalized and F-functionalized Ti_2N with LiPS using first principles calculations. They found that both Ti_2NO_2 and Ti_2NF_2 showed moderate LiPS adsorption energies [79]. The anchoring behavior of six -O-terminated MXenes to LiPS ($Cr_3C_2O_2$, $V_3C_2O_2$, $Nb_3C_2O_2$, $Hf_3C_2O_2$, $Zr_3C_2O_2$, and $Ti_3C_2O_2$) was also investigated by Li et al. [80]. The results indicated that $Cr_3C_2O_2$ had the strongest anchoring effect with Li_2S_4 and Li_2S_8 (Fig. 7b, c).

Apart from computational simulation study, Soni et al. had prepared N-Ti_3C_2/CNT microspheres by the simple spray drying method with HCl-treated melamine as carbon and nitrogen source, and applied as LSB cathode [144]. MXene nanosheet connects with CNT to form porous and conductive network. It was also found that nitrogen-doped MXene and CNT were effective in LiPS capturing to prevent shuttle effect. As indicated in Fig. 8, the cycling performance of 0.2C and 1C was measured and nitrogen-doped Ti_3C_2/CNT microspheres/S cathode demonstrated initial capacity of 1124.6 mAh g^{-1} and reversible capacity of 1025.3 $mAhg^{-1}$ after 200 cycles which means high capacity retention up to 91.2%. This is much higher than that of nitrogen-doped Ti_3C_2/S cathode (598.5 mAh g^{-1} after 200 cycles, capacity retention: 63.6%). In addition, nitrogen-doped Ti_3C_2/CNTs/S cathode also indicated good cycling stability although this cycling stability difference was more obvious at 1 C (Fig. 8b). Even though nitrogen-doped Ti_3C_2/CNT microspheres/S cathode presented highly stable cycling performance up to 1000 cycles. The cathode delivers initial capacity of 927.5 $mAhg^{-1}$ and reversible capacity of 775.6 mAh g^{-1} after 1000 cycles with low fading rate of 0.016% per cycle.

Impedance analysis was also performed to confirm improved electrochemical characteristics. Nyquist plots present one depressed semicircle and a sloped line before cycling (Fig. 8c), which correspond to charge transfer resistance (Rct) and charge diffusion resistance (W), respectively [137]. Rct was lowest for nitrogen-doped Ti_3C_2/CNT microspheres/S cathode owing to enhanced conductivity. Another semicircle appears at high-frequency region after cycling (Fig. 8d). It was suggested that this is due to the resistance of insulating Li_2S layers (Rg) originated from unreacted chemicals during electrochemical reaction [138]. In any case, nitrogen-doped Ti_3C_2/CNT microspheres/S cathode demonstrated lowest resistance among 3 types of electrodes, indicating an efficient electrochemical redox reaction owing to high conductivity and positive interaction effects between CNT and MXene as sulfur host materials.

In short, MXenes possess advantageous properties including metallic conductivity, mechanical toughness, structural diversity, and strong LiPS adsorption. This not only promotes redox reaction kinetics through high electron mobility but also suppresses the shuttle effect through functionalized MXene terminations. In addition, its partially functionalized terminations enable MXene to retain metallic properties that two-dimensional materials such as graphene cannot possess. Thus, MXenes are a promising material for LSBs.

Sulfur-graphene, carbon nanotube composites

As one of a kind carbonaceous material, graphene has been intensively studied as an intermediate LSB layer to overcome the aforementioned problems of the LSB, owing to its large surface area, good chemical stability, and excellent electrical conductivity. Graphene-based materials have been receiving considerable attention in recent years. The application of graphene-based materials in LSB production has mainly involved graphene, heteroatom-doped graphene,

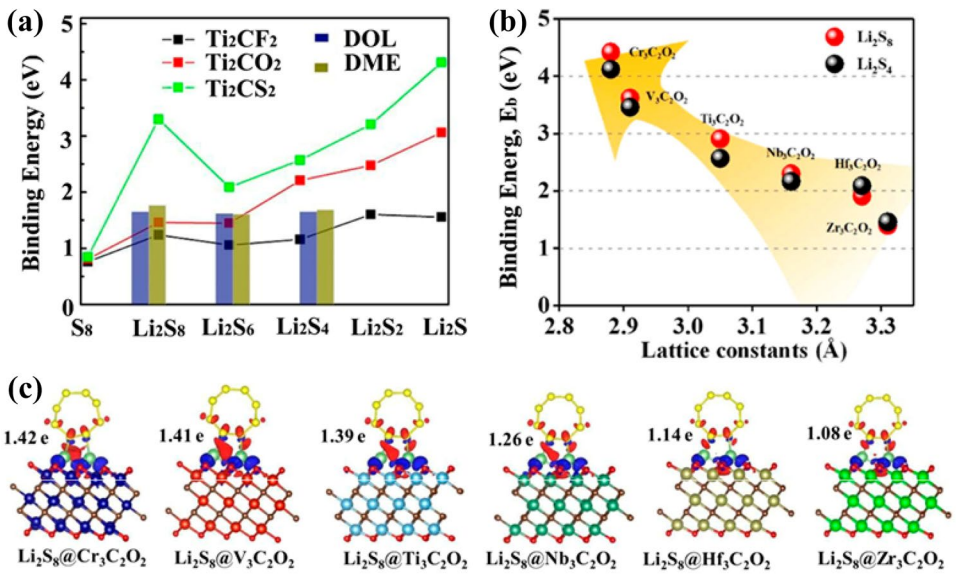

Fig. 7 **a** Comparison of binding energies between lithium polysulfide and $Ti_2CT_x$with different surface terminations [78]. The binding energies (**b**) and differential charge density (**c**) for Li_2S_8 and Li_2S_4 as a function of lattice constants of $M_3C_2O_2$ (M = Zr, V, Ti, Nb, Hf, and Cr) MXenes [80]

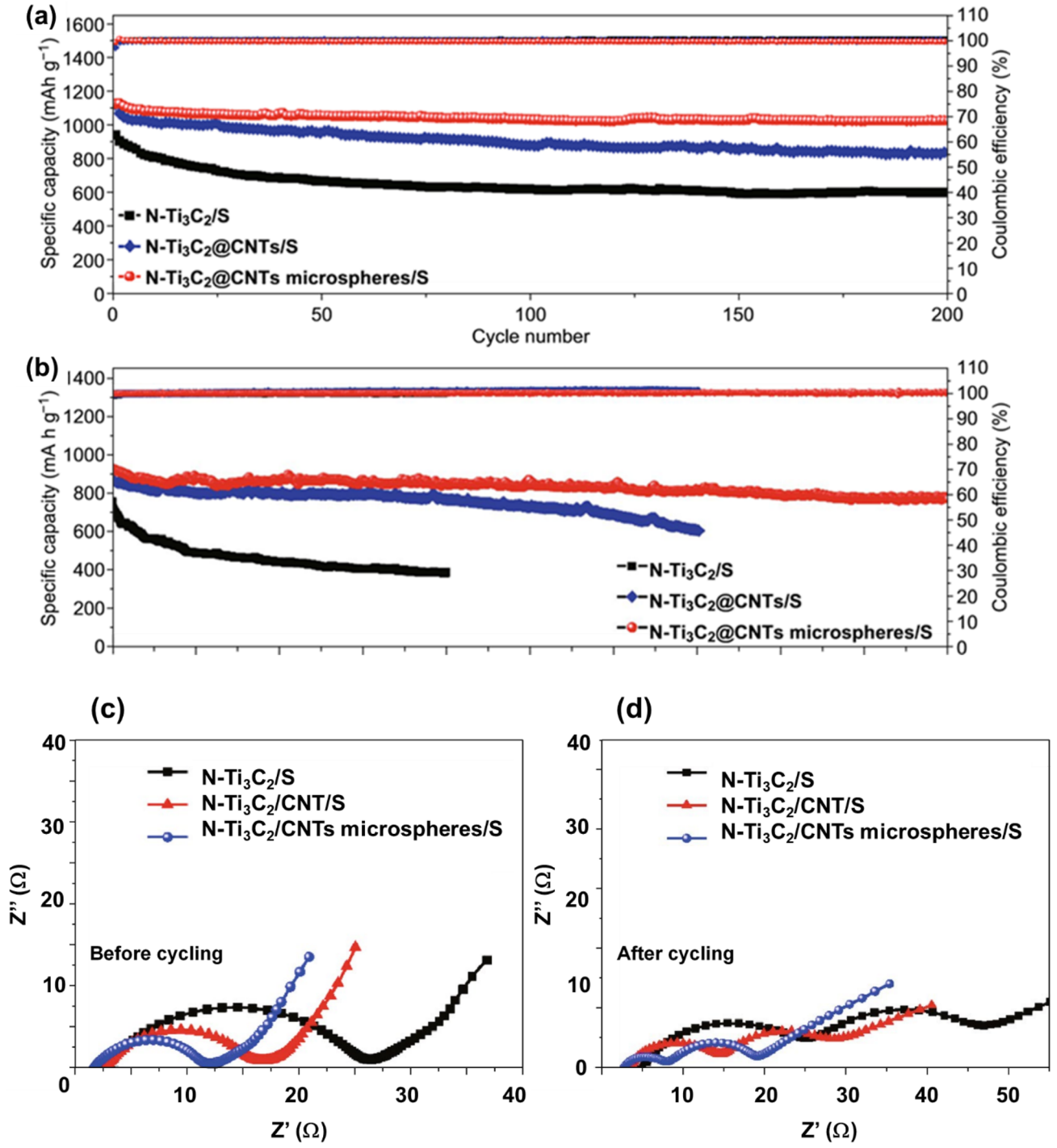

Fig. 8 Cycling performance of three type of cathodes at (**a**) 0.2 C and (**b**) 1 C. EIS spectra of sulfur cathodes (**c**) before and (**d**) after cycles

and graphene-based composite materials [81]. Highly symmetrical hexagonal honeycomb carbon structure of graphene has gained a wide array of attention owing to its unique structure and excellent physicochemical properties, which includes excellent conductivity. This is mainly because the π-electrons derived from the pz orbital of the adjacent atom in the plane move freely, endowing graphene with excellent electrical and thermal properties [82, 83]. Owing to these excellent properties, graphene also has been studied as cathode materials for LSBs.

LSB with multidimensional cathode architecture consisting of nano-sulfur, graphene nanoplatelets, and multi-walled

carbon nanotubes (MWCNT) was prepared and its electrochemical properties were investigated. Prepared LSB exhibited a high specific capacity (1067 mAh g^{-1} at 50 mA g^{-1}), rate performance (539 at 1 A g^{-1}), Coulombic efficiency (~95%), and cycling stability (726 mAh g^{-1} after 100 cycles at 200 mA g^{-1}). These high electrochemical performances were suggested to be due to the encapsulation of nano-sulfur between the individual layers of graphene nanoplatelets with high electronic conductivity, and effective LiPS trapping by multi-wall carbon nanotube [84]. Sulfur cathodes containing 5 wt% (GNS58-CNT5) and 10 wt% (GNS58-CNT10) of MWCNT compositions were tested and compared with GNS58 (graphene 58%—sulfur-CNT hybrid cathode) (Fig. 9a). As predicted, the CBS58 (sulfur-carbon composites containing 58% of carbon particles and sulfur nanoparticles) exhibited the lowest rate performance due to the use of carbon black instead of graphene. GNS58 (MWCNT-free cathode) delivered a lower specific capacity than those of GNS58-CNT5 and GNS58-CNT10 at identical testing conditions. The influence of the MWCNT additive on the long-term cycling stability was tested at a current density of 200 mA g^{-1} (Fig. 9b). GNS58 showed poor capacity retention than MWCNT contained cathode. It is obvious that MWCNT additive improved specific capacities, rate performance, Coulombic efficiency and cycling stability. Electrochemical impedance spectroscopy (EIS) measurements are performed to further study the MWCNT additive influence (Fig. 9c, d). Charge transfer resistances of GNS58 and GNS58-CNT10 electrodes are 75 and 65 Ω, respectively. The improved charge transfer of GNS58-CNT10 can be attributed to enhanced conductivity and contact with the electrolyte solution by adding MWCNT. After 10 times of charge–discharge cycles, Rct of GNS58 increased to 123 Ω, and that of GNS58-CNT10 decreased to 47 Ω. It was deducted that the MWCNT additive effectively trap LiPS which led to reducing shuttling and accumulation of LiPS on the surface, resulted in reducing charge transfer resistance during galvanostatic cycling [84].

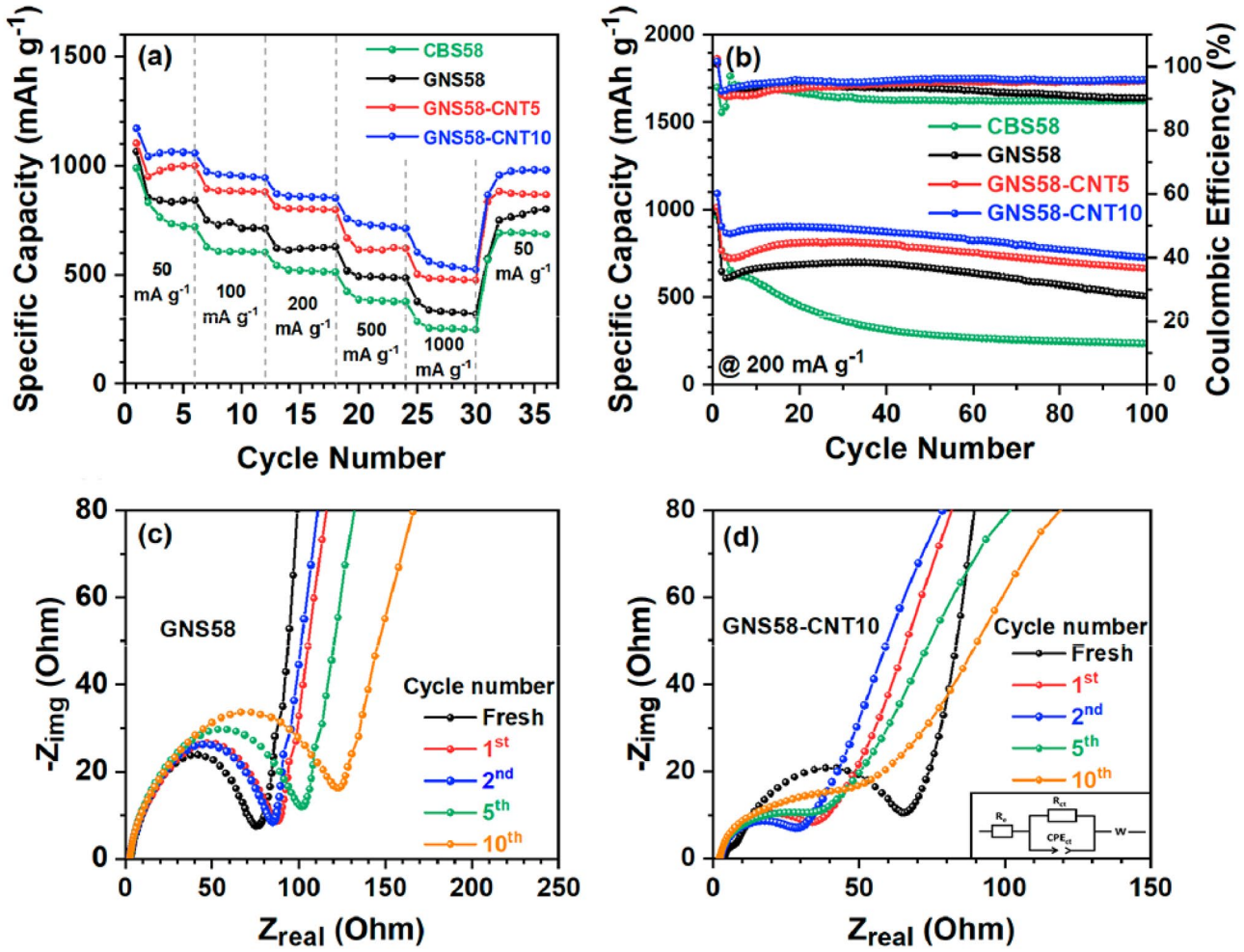

Fig. 9 **a** Galvanostatic rate performance. **b** Cycling performance of GNS58, GNS58-CNT5, and GNS58-CNT10 cathodes. Cole–cole plots of (**c**) GNS58 and (**d**) GNS58-CNT10 cathodes. Inset: equivalent circuit model used for fitting the EIS spectra

Liu et al. reported that carbon or carbon nanotube form composite with graphene oxide through the π-stacking interaction, thus causing carbonaceous materials to stably disperse and fractionate in aqueous media. They had also presented that graphene oxide sheets are prone to stabilize carbon nanotube with larger diameters. In addition, they suggested that hydrophilic oxygen groups of graphene oxide were effective for dispersing in water [85]. On the other hand, Wang et al. studied the synthesis of a graphene-sulfur composite material by wrapping polyethyleneglycol (PEG)–coated submicron sulfur particles with oxidized graphene oxide sheets modified by carbon black [86]. Oxidized graphene oxide was used to prepare sulfur composite materials and carbon black nanoparticles were loaded onto graphene oxide by sonication method in order to increase the graphene oxide sheets conductivity and the final composite material. This composites were further dispersed in water favorably since graphene oxide possess both hydrophobic aromatic parts to interact with carbon black and hydrophilic parts (oxygen functional groups) for dispersion in water as suggested above. Sulfur particles were synthesized by reacting sodium thiosulfate with hydrochloric acid in an aqueous solution of surfactant. These materials were then mixed together to make the final sulfur-graphene oxide composite (Fig. 10). PEG and graphene-coated materials were effective in enhancing conductivity, trapping soluble LiPS and against sulfur volume expansion. The resulting graphene-sulfur composite showed high and stable specific capacities up to ~ 600mAh g^{-1} over more than 100 cycles [86]. These studies imply that by utilizing useful feature of individual materials such as conductivity, LiPS adsorption, and the dispersibility in the liquid for electrode coating ink, prepared composite materials can perform high LSB electrochemical properties.

Heteroatoms element doping such as nitrogen, boron, phosphorous, and sulfur doping to carbonaceous material is the one of effective method to improve electrochemical properties of graphene. This type of doped graphene demonstrates a variety of characteristics, including ferromagnetism, superconductivity, and certain electrochemical and mechanical properties [87]. Especially the nitrogen atom is considered to be one of the best heteroatom to enhance the electrical conductivity of graphene, together with its surface catalytic properties and the control of local chemical features. This enhancement is deducted to be mainly due to the transfer of electrons from the highly electronegative N atom to the adjacent C atom [88].

Jia et al. prepared nitrogen-doped graphene aerogel (N-GA) by hydrothermal method. Thereafter, sulfur was encapsulated in N-GA by chemical deposition to synthesize sulfur encapsulated in N-GA (N-GA/S) composites. When sulfur content was 75.5%, specific capacity reached 723.9 mAh g^{-1} after 100 cycles at 0.7 C, and the capacity retention rate is up to 87.4% while the Coulombic efficiency still remains 98%. It was inferred that this excellent electrochemical property was due to conductivity enhancement of graphene by nitrogen doping as well as the strong LiPS adsorption ability [89].

Three-dimensional N-doped reduced graphene oxide nanosheets were modified with a uniform distribution of Co–Ni-S nanoparticles to form composite material to be used as a sulfur host material for LSB. Co–Ni-S nanoparticles and composite materials interact with LiPS, whereas graphene enhanced the electrical conductivity. This type of cathode delivered an initial discharge capacity of 1430 mAh g^{-1} at 0.1C and demonstrated 685 mAh g^{-1} at 0.5 C even after 300 cycles, with a Coulombic efficiency of 98% [90].

The B atom is another heteroatom that can create defects in bare graphene so that C atom can modulate the electron donors/receptors which would result in enhancing the electrochemical properties [91]. Boron-doped graphene aerogel was prepared by hydrothermal treatment and applied as cathode for LSBs. Boron was positively polarized in the graphene

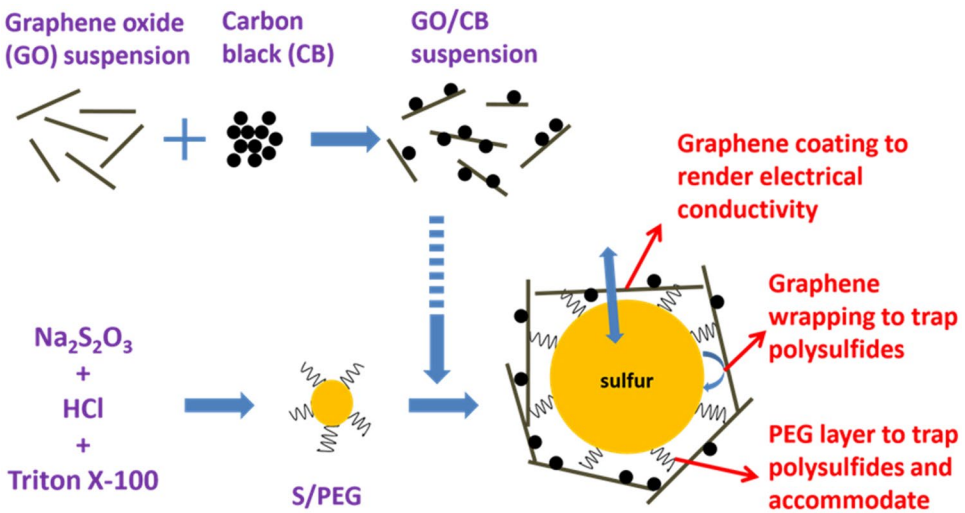

Fig. 10 Schematic of the synthesis steps for a graphene-sulfur composite, with a proposed schematic structure of the composite [87]

framework which resulted in enhanced capturing ability of negative LiPS species. Compared with nitrogen and undoped graphene aerogel, boron-doped graphene-based cathode demonstrated a higher capacity of 994 mAh g^{-1} at 0.2 C after 100 cycles, as well as a superior rate capability [92].

Shi et al. also made boron-doped graphene sheets by electrochemical exfoliation of graphite in a 1.0 mol L^{-1} Li bis(oxalato)borate (LiBOB)/dimethyl methylphosphonate (DMMP) electrolyte. Prepared cathode containing 72.5% of sulfur by this procedure exhibited initial discharge capacity of 1476 mAh g^{-1} at 0.1 C. At 1 C, the capacity of 1018 mAh g^{-1} and excellent retention capability of 838 mAh g^{-1} after 130 cycles were observed. These superior electrochemical properties were suggested to be owing to the few defects and big planar size of cathode, which is helpful for increasing the conductivity and suppressing long-chain LiPS shuttle effect. In addition, the doped boron atoms as active sites could efficiently trap LiPS by chemical adsorption [93].

Sulfur-quantum dot composites

When a solid substance exhibits a distinct variation of optical and electronic properties with a variation of particle size < 100 nm, it can be considered a nanostructure or quantum dot (QD) [94]. QDs are general semiconductor particles a few nanometers in size and have optical and electronic properties that differ from larger particles due to the operation of quantum mechanics. QDs are zero-dimensional relative to the bulk substance, and the limited number of electrons results in discrete quantized energies in the density of states (DOS) [95]. Recently, QDs have attracted extensive attention as materials for electrochemical energy due to their large specific surface area, adjustable size, short ion/electron transport paths, non-toxicity, low cost, adjustable photoluminescence, and easy surface functionalization [96, 97]. The surface of a QD is rich in hetero-atomic functional groups, providing a wide range of active sites. They can be used as composite materials for current collectors and active electrodes, possessing superior ionic conductivity, a high kinetic rate, large capacity, and cycle stability, significantly improving the performance of electrochemical energy storage devices [98–100]. With regard to LSBs, a QD provides an abundance of active sites for the adsorption and localization of LiPS. It can achieve a high sulfur load, thereby reducing LiPS shuttle and the accompanying volume expansion of the sulfur particles.

For example, Han et al. prepared CdS quantum dots carbon nanotube/S composite materials as LSB cathode. Multi-walled CNTs were purified with H_2SO_4/HNO_3 (1:3, volume ratio) at 80 °C. Then after, CdS quantum dot powder was dissolved in hexane and stirred together with purified MWCNT in three necked flask at 80 °C for 5 h. Vacuum freeze-drying method was performed to obtain CNT/CdS quantum dots powder and mixed with sulfur. This type of cathode material demonstrated high LiPS adsorption ability and kinetics reaction owing to synergic catalytic effect of cadmium and heteroatoms. Consequently, the specific capacity was 1237.8 mA h g^{-1} at 0.2C and 918.1 mA h g^{-1} at 2.0C, indicating a high-rate performance. In addition, capacity was 820.6 mA h g^{-1} at 0.5C for over 150 cycles proving high Coulombic efficiency of over 98.0% [101].

ZnO quantum dot–modified reduced graphene oxide was prepared and applied for LSB cathode. Zn foil was immersed in a graphene oxide solution at room temperature. Graphene oxide could be reduced by Zn to form a uniform film on the surface of Zn foil because the reduction potential of Zn/Zn^{2+} is lower than that of reduced graphene oxide/graphene oxide. Then, ZnO nanoparticles deposited on the graphene oxide flakes as a result of the redox reaction. Following HCl etching and heat treatment procedure would make final reduced graphene oxide/ZnO quantum dot composite (Fig. 11). Owing to its catalysis effect, enhanced reaction kinetics, low surface impedance and efficient adsorption of LiPS, prepared ZnO quantum dot–based cathode presented excellent rate capacity even at a high rate of 4C and stable cycle performance. An initial discharge capacity of 998.8 mAh g^{-1} as delivered, of which 73.3% was retained even after 400 cycles at a high rate of 1C [102].

Zhao et al. had synthesized core shell ZnSe quantum dot/CNT/S/$Ni(OH)_2$ and applied as LSB cathode. $Ni(OH)_2$ was prepared in layered form. CNT (carbon nanotube) network decorated with ZnSe quantum dots was supportive materials for sulfur loading and also worked as conductive framework for effective electron and ion transfer. It also had role to suppress LiPS diffusion. Layered $Ni(OH)_2$ as wrinkled capsulation materials was also effective in terms of electron/ion transfer. They are also helpful materials to buffer sulfur expansion and keeping the active materials in cathode. When ZnSe quantum dot/CNT/S/$Ni(OH)_2$ was used as LSB cathode, specific capacity was 1021.9 mAh g^{-1} and 665.0 mAh g^{-1} at 0.2 C and 2 C, respectively. At 0.5C, initial capacity was 926.7 mAh g^{-1} which became 789.0 mAh g^{-1} after 150 cycles. These studies indicate that quantum dots can be promising cathode materials for LSBs [103].

Artchuea et al. synthesized CuZnS quantum dots decorated with nickel–cobalt-sulfide mixed with reduced graphene oxide/oxidized carbon nanotube composites and applied as LSB cathode. This CuZnS quantum dot–based cathode delivered an initial capacity of 1344.18 $mAhg^{-1}$ at 0.1C with Coulombic efficiency of 97.62% which is approximately 1.16 times higher compared to the absence of the Cu–Zn-S quantum dot [104].

CoNiP quantum dot–modified graphene oxide composite was prepared and utilized as a sulfur host in LSBs. CoNiP quantum dot was synthesized a unique solvothermal reaction and subsequent sintering. Uniformly dispersed CoNiP

quantum dots on graphene oxide nanosheets were confirmed by SEM and TEM. Density functional theory (DFT) calculations elucidated the high activity and metallic property of CoNiP quantum dot. Reduced graphene oxide further improved the electronic conductivity of cathode. By combining these 2 materials, prepared LSB exhibited 598.2 mA h g^{-1} at 3C. Cycle performance test elucidated capacity decay rate of 0.08% after 600 cycles at 1C rate [105].

Besides metallic-based quantum dot, Park et al. had introduced graphene quantum dots for LSB cathode and increased sulfur/sulfide utilization in order to enhance electrochemical performance. Graphene quantum dots were synthesized by modified Hummer's method from carbon fiber, H_2SO_4, and HNO_3 as raw materials. The graphene quantum dots improved the structural integrity of the sulfur-carbon electrode composite via its oxygen-rich functional groups. This hierarchical architecture enabled rapid charge transfer while minimizing the loss of lithium polysulfide [106]. They had analyzed graphene quantum dot with various types of microscopic and spectroscopic tools including high-resolution transmission electron image (Fig. 12a, b). Prepared graphene quantum dot was found to be highly polycrystalline (Fig. 12c). Some vibrational modes of oxygen functional groups were clearly observed as -OH at 3434 cm^{-1}, C = O at 1725 cm^{-1}, C-O in 1024–1180 cm^{-1}, and C–O–C at 1200 cm^{-1}. In addition, sp2-hybridized C = C bonds (in-plane stretching) was seen at 1629 cm^{-1} [139]. Sulfur and graphene quantum dot composite materials were also observed with SEM, TEM, and EDS mapping of C, S, and S. One could find that sulfur particles were homogeneously coated with graphene quantum dots (Fig. 12d, e). Such a uniform graphene quantum dot distribution was possible due to their extreme small size, as well as the oxygen functional groups on the particles, which led to electrostatic interactions with sulfur. Raman spectroscopy was also applied and peaks were observed at (D and G at 1350 and 1590 cm^{-1}) for carbon and (the four characteristic peaks below 600 cm^{-1}) for sulfur (Fig. 12d, e) [140]. In addition, they have prepared graphene quantum dot/S/carbon black composite material via van der Walls interactions [141]. It was confirmed that carbon blacks were tightly bound to graphene quantum dot/S composite and C, O, and S were homogenously distributed (Fig. 12g). Figure 12 h and i show the graphene quantum dot is uniformly distributed on the sulfur surface and bonded to carbon black strongly. In order to confirm graphene quantum dot/S/carbon black composite stability, sulfur was dissolved by CS2 solution from graphene quantum dot/S/carbon black composite. It was found that even without the sulfur, composite structure was robust and remain intact (Fig. 12j–l). Owing to their robust nature of graphene quantum dot/S/carbon black composite materials, when used as LSB cathode, they presented superior cyclability and stable Coulombic efficiency compared with sulfur/carbon black cathode. A discharge capacity reached ~ 1000 mAh g^{-1} even after 100 cycles. In contrast, sulfur/carbon black cathode indicated a discharge capacity of only 459.6 mAh g^{-1}. It was also elucidated that the C-S bonding supplied by graphene quantum dot was also critical point to enhance LSB performance. The schematic illustration in Fig. 13 presents a conventional LSB with metallic lithium anode and sulfur-carbon composite cathode. The structure of the cathode had a great impact on the irreversible loss of high-order LiPS during repeated LSB charge–discharge cycles. When graphene quantum dots were applied as cathode, because graphene quantum dots possess both hydrophobic aromatic and hydrophilic defective parts, they could interact with carbon and sulfur,

Fig. 12 Materials characterization of GQDs-S/CB and S/CB composites. **a**, **b** High-resolution TEM images of GQDs; the inset shows a histogram of the GQD size distribution. **c** FT-IR spectra of GQDs and CB. The peaks in this figure correspond to the various functional groups in the GQDs and CB. SEM images of (**d**) GQDs-S and (**g**) GQDs-S/CB. **e** High-resolution transmission electron microscope (HRTEM) images of the GQDs-S composites and GQD pattern (yellow circle). A Moiré pattern (red circle) is clearly visible in these TEM images, which was created by a superposition of the GQDs and S crystalline lattices. **f** Raman spectra of GQDs-S and GQDs-S/CB composites, which show that the GQDs were formed on the sulfur particles. The strong peaks at 218.16 and 472.75 cm^{-1} arise from sulfur, and the D (disorder) and G (graphitic) peaks arise from the GQDs. Schematic diagrams show (**h**) the structure and (**i**) the magnified structure of GQDs-S/CB. **j**, **k** HRTEM images and (**l**) SEM image of the shell structures of GQDs-S/CB after rinsing with a CS2 solution

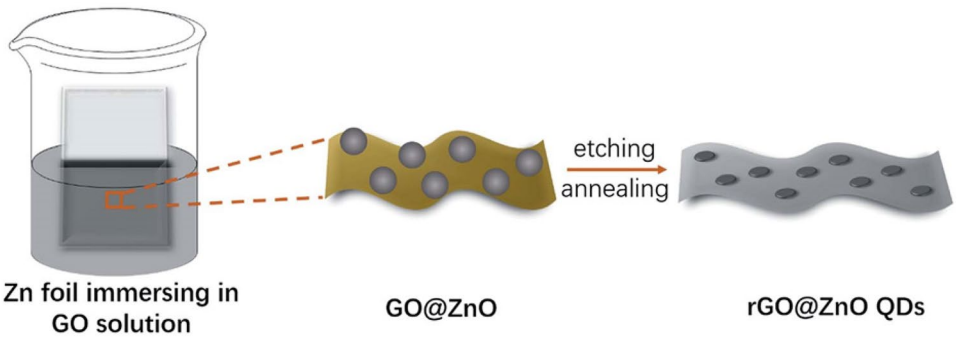

Fig. 11 Schematic illustration of the synthesis of rGO@ZnO QDs

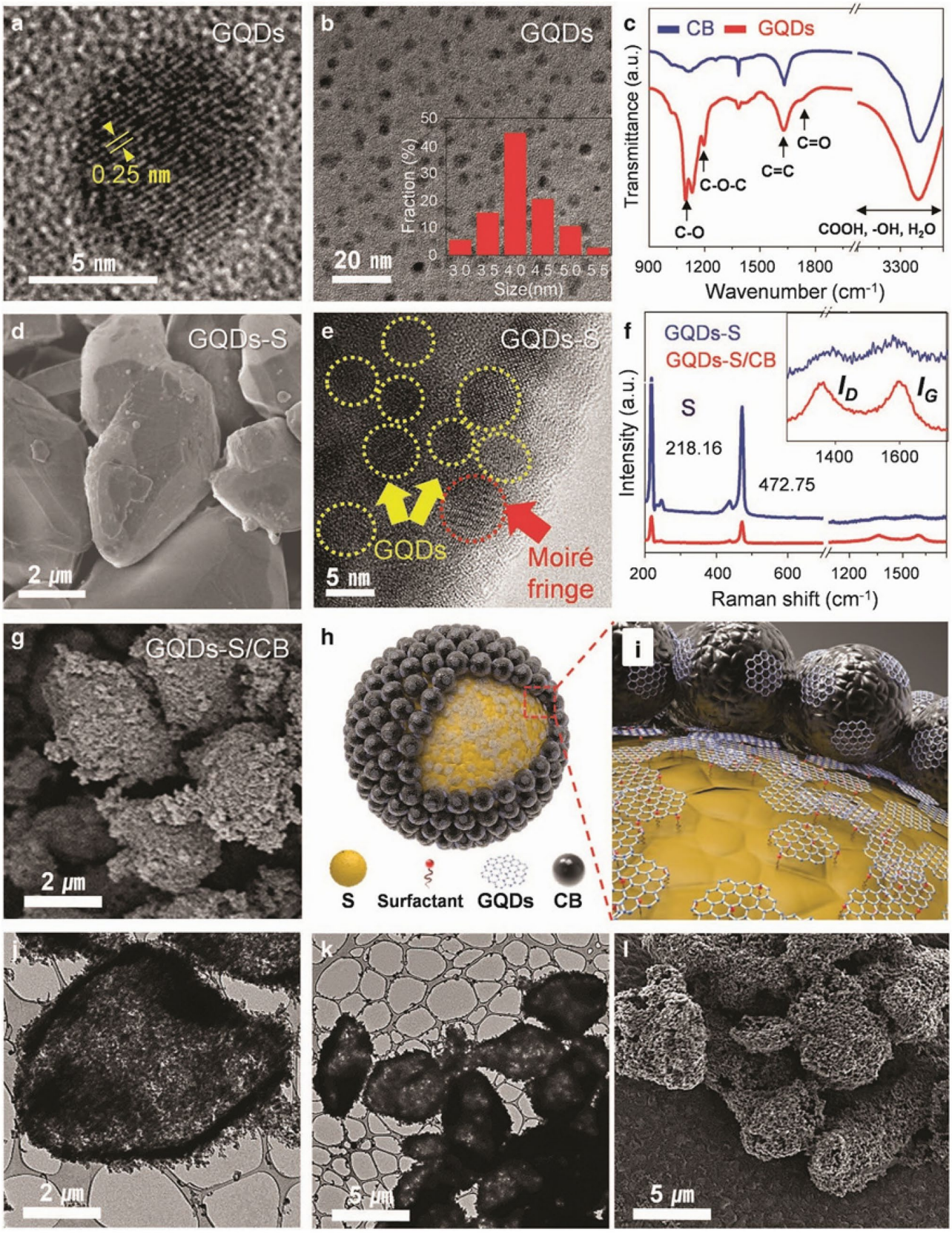
a
GQDs
0.25 nm
5 nm
b
GQDs
Fraction (%)
50
40
30
20
10
0
3.0 3.5 4.0 4.5 5.0 5.5
Size(nm)
20 nm
c
CB
GQDs
Transmittance (a.u.)
C-O
C-O-C
C=C
C=O
COOH, -OH, H2O
900 1200 1500 1800 3300
Wavenumber (cm-1)
d
GQDs-S
2 μm
e
GQDs-S
GQDs
Moiré fringe
5 nm
f
GQDs-S
GQDs-S/CB
S
218.16
472.75
ID
IG
1400 1600
Intensity (a.u.)
200 400 600 1200 1500
Raman shift (cm-1)
g
GQDs-S/CB
2 μm
h
S
Surfactant
GQDs
CB
i
j
2 μm
k
5 μm
l
5 μm

respectively [142]. Owing to these natures, graphene quantum dot can capture LiPS effectively to improve LSB electrochemical performance.

In summary, QDs are an interesting potential material for LSB cathodes owing to their size, extremely large surface area, and quantity of surface functional sites.

Sulfur-metal organic framework composites

Metal organic frameworks (MOFs) have been attracting increasing attention as a possible promising material for batteries. The typical MOF is an organic–inorganic hybrid material formed through the self-assembly of a coordination bond having a central metal ion and an organic ligand. MOF research has grown remarkably over the years [107–109]. Compared with weak bonds, such as van der Waals bonds and hydrogen bonds, MOFs have a stronger coordination bond energy (generally 60–350 kJ mol^{-1}), which endow them a certain stability. Furthermore, the structure and physical and chemical properties of MOFs are highly customizable so that researchers have created more than 20,000 types of MOFs so far, and that number is still growing [110]. This is possible because the use of different center metal ions forms a wide variety of MOF compounds with different organic ligands such that the number of possible combinations is enormous [111–113]. The research of on MOF applications has included drug delivery systems for biomedical use [114], gas storage and separation [115], catalysis [116], water treatment [117], and more recently, in the field of electrochemistry [118, 119]. The fixation and anchoring of sulfur and LiPS by MOFs are possible due to their large pore volumes, adjustable structures, and extremely high specific surface area as well as their customizability which would results in promoting LSB performance. These are the main reasons for applying MOFs to LSBs [120, 121].

Gao et al. synthesized large surface area mesoporous chromium MIL-101 (Cr) metal organic framework by hydrothermal method and prepared composite material with CNT as the host of sulfur for LSB cathode. MIL-101/CNT/S cathode demonstrated the excellent electrochemical performance. Especially when the weight of CNT is 5% against the weight of pure MIL-101 (Cr), cathode delivered an initial discharge capacity of 1236.7 mAh g^{-1} at 0.1 C and capacity retention rate reaches 53.4% after 200 cycles. Discharge capacity was multiple times higher than when MIL-101 (Cr)/S cathode, indicating favorable combination of CNT and MOF [122].

Different from just simply mixing MOFs with sulfur for designing sulfur cathodes, Liu et al. took another strategy to improve the cycle stability by introducing covalently bonded sulfur in MOFs. Compared with an LSB using the simple blend of sulfur and MOFs as the cathode, LSB with the cathode consisting of sulfur covalently connected with the MOF exhibited outstanding long-cycling stability. Specifically, the LSB with CNT/UIO66-S delivered high capacity retention of 80.19% even after 900 cycles at the current of 2C. It was suggested that introducing sulfur in MOFs by covalent connection may be new strategy to further improve LSB performance compared to just simply mixing MOF with sulfur [123].

Chen et al. studied the two-dimensional porphyrin-like square MOF-based LSB cathode with first principle DFT calculation. The DFT results show that among 7 kinds of transition-metal organic framework (TM-MOF) they have studied, V-MOF and Ru-MOF were able to demonstrate remarkable chemical interactions with S_8 and LiPS in both vacuum and in electrolytic solvents, demonstrating higher capturing performance compared to other transition metal–based MOF. When V-MOF-based cathode was applied, prepared LSB presented a relatively constant open-circuit voltage of about 1.92

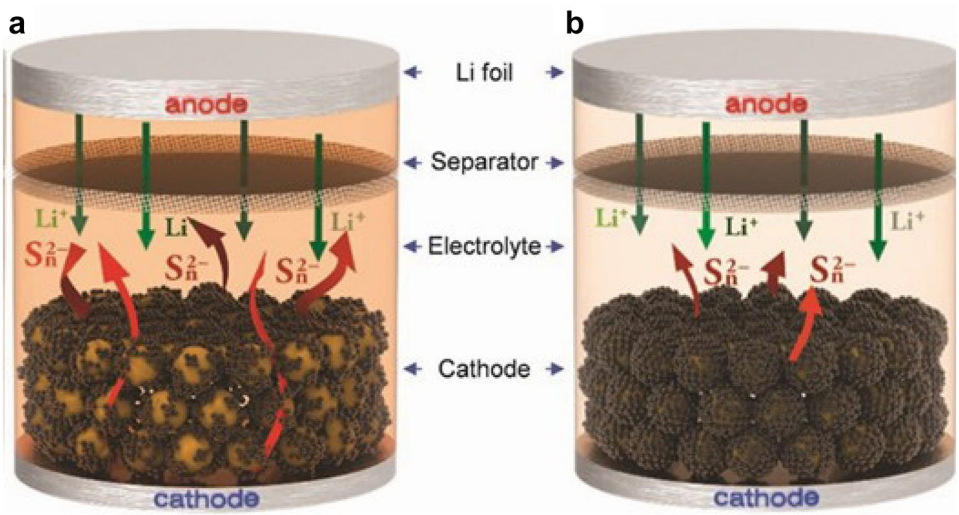

Fig. 13 Schematic diagrams of sulfur/carbon black and graphene quantum dot/sulfur/carbon black in LSB. The sulfur (yellow) was wrapped with carbon black and graphene quantum dot. LiPS were dissolved into the solvent and the color changed to orange

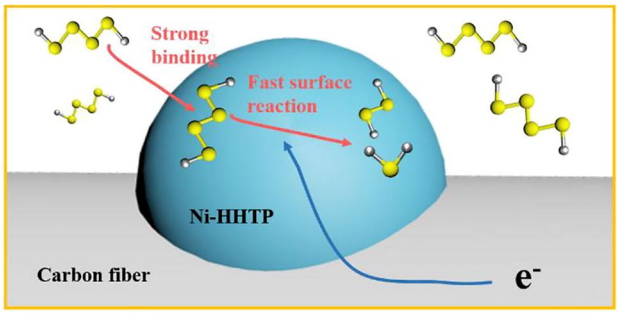

Fig. 14 Conductive MOFs which possess strong LiPS adsorption and excellent electronic conductivity are conducive to promoting LiPS transformation in LSB

to 1.95 V. In addition, volume expansion of V-MOF during discharge was elucidated to be about 34%, much smaller than 80% for solid sulfur. The band structure and density of states of V-MOF were suggested to be metallic properties or a small band gap for bare surface. These results indicate that two-dimensional (2D) V-MOFs can behave as high-performance cathode material with enhanced capturing influence to block LiPS dissolution in order to reduce shuttle effect to attain excellent LSB performance [124].

Qu et al. also had applied first principle DFT calculation for MOF-based LSB cathode study. They applied cobalt-metal organic framework (Co-MOF) to prepare composite materials with sulfur to prepare LSB cathode. They had confirmed higher capacity retention of Co-MOF-S cathode than pure sulfur cathode by 87.18% after 100 cycles at 0.1C. Qu et al. had investigated detail mechanism with XPS and DFT calculation to confirm the covalent bond connection between Co-MOF and S. They had found that the C 1 s spectrum of the Co-$MOFS_2$ material indicated three peaks with binding energies of 284.5, 285.7, and 288.6 eV that correspond to carbon atoms in different functional groups of the MOF structure. There were also fourth peak with binding energy of 286.5 eV which was suggested to be related to the structure of MOF as a result of sulfur binding. They had confirmed that this 286.5 eV peak was absent with pristine Co-MOF XPS result. DFT calculation elucidated that this 286.5 eV as additional fourth peak is suggested to be assigned to the $[O=C-S]^-$ group [125].

When sulfur is embedded in the pores of an MOF, the MOF then plays an important role in the packaging and conversion of the sulfur and sulfide. However, when MOFs are used as active substances for electrode materials, it might be more ideal to combine MOFs with conductive polymers because the intrinsic nature of MOFs is insulator. Jiang et al. studied a new method to promote the conductivities of MOFs by 5 to 7 magnitudes. Their method combines the polarity and porosity advantages of MOFs with the conductive polymers, polypyrrole (ppy), and used as LSB cathode. The electrochemical performance of these ppy-sulfur-MOF composite was superior to their MOF and ppy counterparts specifically at high charge–discharge rates. As a result, the ppy-sulfur-in-PCN-224 electrode delivered a high capacity of 670 and 440 mAh g^{-1} at 10.0 C after 200 and 1000 cycles, respectively [126].

Wang et al. had introduced conductive MOFs to promote LiPS transformation owing to its excellent conductivity. A nickel-catecholates–based conductive MOF, Ni-HHTP (HHTP = 2,3,6,7,10,11-hexahydroxytriphenylene), was designed to control the surface chemistry of self-supported carbon paper for LSB cathode. Owing to porous structure

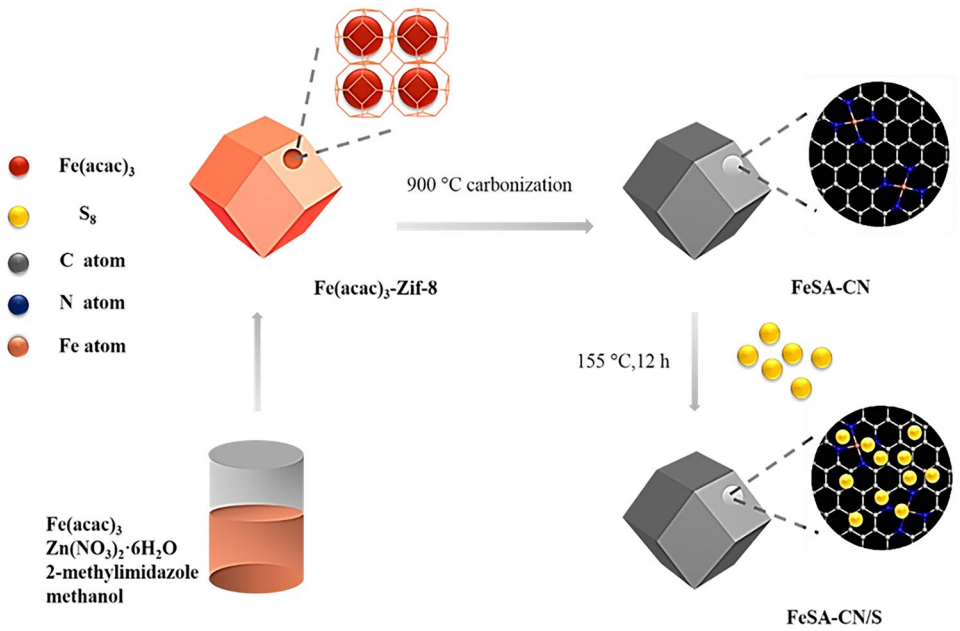

Fig. 15 Synthesis procedure of iron single-atom catalyst/nitrogen-doped carbon/sulfur composite

Table 1 Comparative performances of LSB with different cathode

Sulfur host material	Sulfur content (wt %)	Current density (C, 1675 mAg^{-1})	Cycle number	Discharge capacity ($mAhg^{-1}$)	Capacity retention (Fadeing rate)	Reference
Metal oxide/sulfur						
MnO_2	75		2000	1300	0.036%/cycle	[34]
WO_{3-x}		4	100	693.2	0.049%/cycle	[35]
V_2O_5	70		1000		0.049%/cycle	[36]
$LaMnO_{3-\delta}$		0.1	1346	400	0.1/cycle	[37]
CeO_2/MMNC nanospheres	63.6	1	500	836	0.076%/cycle	[38]
SnO_2/reduced graphene oxide		1	200	734		[39]
Hollow-CNT/S/ZrO2		10	200	870		[40]
TiO_2 nanofibers/S			50	530	0.8%/cycle	[41]
α-Fe_2O_3		0.3	1000	1571	0.049%/cycle	[42]
Ti_4O_7/S	70	0.2	100	1070	0.12%/cycle	[43]
Metal sulfide/sulfur						
CoS_2		0.5	2000	1368	0.034%/cycle	[46]
WS_2		0.5	350	590		[47]
MoS_2			1000		0.025%/cycle	[48]
Metal carbide/sulfur						
W_2C		0.2, 1	500	1200 (0.2C) 605 (1C)	0.06%/cycle	[51]
WC		5		789		[54]
B_4C nanowire	70	4	500		0.04%/cycle	[55]
Metal nitride/sulfur						
VN		1, 15	200, 500	790 mAh (1C) 145.2 (15C)		[56]
CN	66.7	0.5	100	828.4		[57]
TiN nanoparticles/graphene		0.1	180	1229	0.07%/cycle	[59]
$Co_{5.47}N_x$-C		0.5		850		[60]
MXene/sulfur						
Ti_2C	70	0.2	400	1200	0.05%/cycle	[74]
Nitrogen-doped Ti_3C_2/CNT			1000	927.5	0.016%/cycle	[144]
Graphene, carbon nanotube/sulfur						
Graphene-sulfur-CNT		200	100	726		[84]
Nitrogen-doped graphene aerogel	75.5	0.7	100	723.9	0.13%/cycle	[89]
N-doped reduced graphene oxide nanosheets		0.5	300	685		[90]
3D boron-doped graphene aerogel		0.2	100	994		[92]
Boron-doped graphene sheet	72.5	1	130	1018	1.38%/cycle	[93]
Quantom dot/sulfur						
Cd/S quantum dot		0.5	150	820.6		[101]
ZnO quantum dot/graphene oxide	73.3	1	400	998.8		[102]
ZnSe quantum dots (QDs) and layered Ni(OH)2		0.5	150	926.7	0.1%/cycle	[103]
CoNiP quantum dot -rGO/S		3	600	598.2	0.08%/cycle	[105]
Graphene quantum dot/carbon black			1000	100		[106]
Metal organic framework/sulfur						
MIL-101/carbon nanotube		1	200	1236.7	0.23%/cycle	[122]
UiO 66/carbon nanotube		1	450	608	0.017%/cycle	[123]
The ppy-S-in-PCN-224		10	1000	440		[126]
Single-atom catalyst derived from MOF		4	500	605	0.06%/cycle	[129]

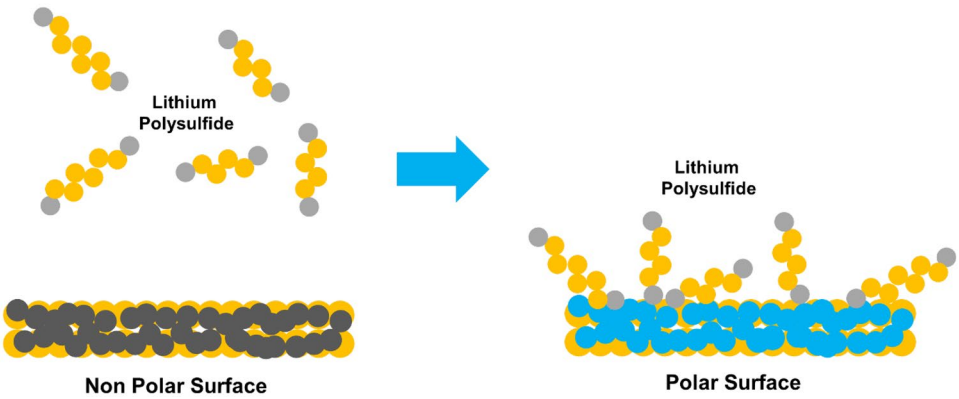

Fig. 16 Schematic illustration of the comparison effect of LiPS on LSB cathode with non-polar and polar surface

and high conductivity of conductive MOF, Ni-HHTP–based cathode was able to strengthen the adsorption of LiPS and accelerated the reaction kinetics which resulted in enhancing LSB electrochemical performance (Fig. 14) [127].

Creating heteroatoms (e.g., N, S, B, P) doped carbon with MOF is one of another effectively way to improve LSB cathode performance. Chen et al. prepared MOF-derived nitrogen-doped porous carbon which was anchored on graphene sheets and applied as a sulfur host for LSB cathode. It was found out that the large surface area of nitrogen-doped carbon material originated from MOF nature was also effective regarding immobilizing LiPS. In their study, highly conductive graphene offered a conductive network to further promote fast charge transfer, which resulted in enhancing LSB performance. Eventually, MOF-derived cathode delivered a high specific capacity of 1372 mAh g^{-1} with good cycling stability over 300 cycles [128].

Furthermore, single-atom catalyst was applied to LSB cathode. Nitrogen-rich MOF-derived carbon modified with an iron single-atom catalyst was prepared and applied as LSB cathode. Iron (III) acetylacetonate, zinc nitrate hexahydrate, and 2-methyl imidazole were used as raw materials to synthesize iron contained ZIF-8. It was further carbonized in inert atmosphere at 900 °C and combined with sulfur (Fig. 15). Synergetic influence of iron single-atom catalyst and nitrogen-doped porous carbon considerably enhanced the electrochemical performance and prepared LSB indicated a specific capacity of 1123 mAh g^{-1} at 0.2C, and exhibited an excellent rate performance of 605 mA h g^{-1} at 4.0C with an ultralow capacity fading rate of 0.06% per cycle for 500 cycles. They had shown new strategy to combine the function of a nanoporous material host and single-atom catalyst for LSB cathode [129].

As above, we have looked at the LSB performance especially depending upon what type of cathode material is applied and summarized in Table 1. Compared to non-polar carbonaceous materials in general, polar material in the table was more preferable in terms of LiPS capturing and demonstrated better LSB electrochemical performance. Each materials have advantage and disadvantage. However, combining those materials or preparing conductive carbon-based composite materials is also important factors to enhance properties such as cathode conductivity and stability.

The author's group has enhanced the capacity and cyclic stability of an LSB by optimizing the cathode structure and electrolyte composition, as well as the separator [130]. For the cathode, we applied silicon as a coupling agent to improve the adhesive force between the cathode ink and the cathode aluminum base. We also utilized a polar material surface to enhance adsorption of LiPS to suppress the shuttle effect (Fig. 16) [131]. For the separator, we coated a MOF-derived ink to improve cyclic stability. Details will be provided in our forthcoming paper.

Conclusions

We have discussed the advantages and drawbacks of LSBs and possible strategical electrochemical property enhancements that can be obtained from the selection of the cathode material. Metal oxides, carbides, nitrides, MXenes, graphene, carbon nanotube, quantum dots, and metal organic frameworks were all considered. One important point raised was that polar material should be preferred because carbonaceous materials possess non-polar surface in general. This will improve adsorption of LiPS and suppress the shuttle effect. Conductivity was also another critical point in order to obtain LSB cathode with high electrochemical performance. It should also be realized the structure of the electrode and in some case, electrolyte (LiPS affinity, reactivity to lithium metal, dielectric constant, viscosity, molecular structure of electrode, etc.) can critically affect the rate of each of the electrochemical reaction steps inside LSB. Even though, by optimizing the material and combining it with sulfur, LSBs should prove themselves as a practical battery device and become the post-lithium-ion battery.

Acknowledgements The author wishes to express thanks to Dr. Hideki Yoshioka, Mr. Koji Yokokawa, Mr. Katsuji Konishi, and Mr. Yoshiyuki Nakano for their helpful discussions.

Declarations

Conflict of interest The author declares no competing interests.

References

1. Wild M, O'Neill L, Zhang, Purkayastha R, Minton G, Marinescu M, Offer GJ (2015) Lithium sulfur batteries, a mechanistic review. Energy Environ Sci 8:3477–3494. https://pubs.rsc.org/en/content/articlelanding/2015/ee/c5ee01388g
2. Pan H, Cheng Z, He P, Zhou H (2020) A review of solid-state lithium–sulfur battery: ion transport and polysulfide chemistry. Energy Fuel 34(10):11942–11961. https://doi.org/10.1021/acs.energyfuels.0c02647
3. Mori R (2020) Recent developments for aluminum–air batteries. Electrochem Energy Rev 3:344–369. https://doi.org/10.1007/s41918-020-00065-4
4. Manthiram A, Fu Y, Chung SH, Zu C, Su YS (2014) Rechargeable lithium - sulfur batteries. Chem Rev 114(23):11751–11787. https://doi.org/10.1021/cr500062v
5. Xu G, Ding B, Pan J, Nie P, Shen L, Zhang X (2014) High performance lithium–sulfur batteries: advances and challenges. J Mater Chem A 2:12662–12676. https://pubs.rsc.org/en/content/articlelanding/2014/ta/c4ta02097a
6. Kang W, Deng N, Ju J, Li Q, Wu D, Ma X, Li L, Naebe M, Cheng B (2016) A review of recent developments in rechargeable lithium–sulfur batteries. Nanoscale 8:16541–16588. https://pubs.rsc.org/en/content/articlelanding/2016/nr/c6nr04923k
7. Lopez CV, Maladeniya CP, Smith RC (2020) Lithium-sulfur batteries: advances and trends, Electrochem 1:226–259. https://www.mdpi.com/2673-3293/1/3/16
8. Feng S, Fu ZH, Chen X (2022) A review on theoretical models for lithium–sulfur battery cathodes. InfoMat 4:e1230–e1254. https://doi.org/10.1002/inf2.12304
9. Lin H, Yang L, Jiang X, Li G, Zhang T, Yao Q, Zheng GW, Lee JY (2017) Electrocatalysis of polysulfide conversion by sulfur-deficient MoS_2 nanoflakes for lithium–sulfur batteries. Energy Environ Sci 10:1476–1486. https://pubs.rsc.org/en/content/articlelanding/2017/ee/c7ee01047h
10. Luo C, Huc E, Gaskell KJ, Fan X, Gao T, Cui C, Ghose S, Yang XQ, Wang C (2020) A chemically stabilized sulfur cathode for lean electrolyte lithium sulfur batteries. PNAS 117(26):4712–4720. https://doi.org/10.1073/pnas.2006301117
11. Manthiram A, Chung S, Zu C (2015) Lithium-sulfur batteries: progress and prospects. Adv Mater 27:1980–2006. https://pubmed.ncbi.nlm.nih.gov/25688969/
12. Chen L, Shaw LL (2014) Recent advances in lithium–sulfur batteries. J Power Sources 267:770–783. https://www.sciencedirect.com/science/article/abs/pii/S0378775314008040
13. Fang R, Zhao S, Sun Z, Wang DW, Cheng HM, Li F (2017) More reliable lithium - sulfur batteries: status, solutions and prospects. Adv Mater 29(48):1606823. https://doi.org/10.1002/adma.201606823
14. Sun Y, Zheng L, Yang Y, Qian X, Fu T, Li X, Yang Z, Yan H, Cui C, Tan W (2020) Metal–organic framework nanocarriers for drug delivery in biomedical applications. Nano-Micro Letters 12:103–131. https://doi.org/10.1007/s40820-020-00423-3
15. Liu Y, Cui C, Liu Y, Liu W, Wei J (2020) Application of MoS_2 in the cathode of lithium sulfur batteries. RSC Adv 10:7384–7395. https://pubs.rsc.org/en/content/articlepdf/2020/ra/c9ra09769d
16. Hagen M, Hanselmann D, Ahlbrecht K, Maca R, Gerber D, Tübke J (2015) Lithium–sulfur cells: the gap between the state-of-the-art and the requirements for high energy battery cells. Adv Energy Mater 5:1401986. https://doi.org/10.1002/aenm.201401986
17. Cleaver T, Kovacik P, Marinescu M (2018) Commercializing lithium sulfur batteries: are we doing the right research? J Electrochem Soc 165(1):A6029-A6033. https://doi.org/10.1149/2.0071801jes/pdf
18. Waluś S, Barchasz C, Bouchet R, Leprêtre JC, Colin JF, Martin JF, Elkaïm E, Baehtz C, Alloin F (2015) Lithium/sulfur batteries upon cycling: structural modifications and species quantification by in situ and operando X-ray diffraction spectroscopy. Adv Energy Mater 5(16):1500165. https://doi.org/10.1002/aenm.201500165
19. Barghamadi M, Best, AS, Bhatt AI, Hollenkamp AF, Musameh M, Ress RJ, Rüther T (2014) Lithium–sulfur batteries—the solution is in the electrolyte, but is the electrolyte a solution? Energy Environ Sci 7:3902–3920. https://pubs.rsc.org/en/content/articlelanding/2014/ee/c4ee02192d
20. Rinkel BLD, Hall DS, Temprano I, Grey CP (2020) Electrolyte oxidation pathways in lithium-ion batteries. J Am Chem Soc 142(35):15058–15074. https://doi.org/10.1021/jacs.0c06363
21. Zoski VG (2006) Handbook of electrochemistry. Elsevier: Amsterdam. The Netherlands. https://www.elsevier.com/books/handbook-of-electrochemistry/zoski/978-0-444-51958-0
22. Luo J, Lee R, Jin J, Weng YT, Fang CC, Wu NL (2017) A dual-functional polymer coating on a lithium anode for suppressing dendrite growth and polysulfide shuttling in Li–S batteries. Chem Commun 53:963–966. https://pubs.rsc.org/en/content/articlelanding/2017/cc/c6cc09248a
23. McCloskey BD (2015) Attainable gravimetric and volumetric energy density of Li–S and Li ion battery cells with solid separator-protected Li metal anodes. J Phys Chem Lett 6:4581–4588. https://doi.org/10.1021/acs.jpclett.5b01814
24. Jeschull F, Brandell D, Edström K, Lacey MJ (2015) A stable graphite negative electrode for the lithium–sulfur battery. Chem Commun 51:17100–17103. https://pubs.rsc.org/en/content/articlelanding/2015/cc/c5cc06666b
25. Krause A, Dörfler S, Piwko M, Wisser FM, Jaumann T, Ahrens E, Giebeler L, Althues H, Schädlich S, Grothe J, Jeffery A, Grube M, Brückner J, Martin J, Eckert J, Kaskel S, Mikolajick T, Weber WM (2016) High area capacity lithium-sulfur full-cell battery with prelitiathed silicon nanowire-carbon anodes for long cycling stability. Sci. Rep. 6:27982 – 27993. https://www.nature.com/articles/srep27982.pdf
26. Park MG, Lee DH, Jung H, Choi JH, Park CM (2018) Sn-based nanocomposite for Li-ion battery anode with high energy density, rate capability, and reversibility. ACS Nano 12(3):955–2967. https://doi.org/10.1021/acsnano.8b00586
27. Piwko M, Kuntze T, Winkler S, Straach S, Hartel P, Althues H, Kaskel S (2017) Hierarchical columnar silicon anode structures for high energy density lithium sulfur batteries. J Power Sources

351:183–191. https://www.sciencedirect.com/science/article/abs/pii/S0378775317303786
28. Cao R, Xu W, Lv D, Xiao J, Zhang JG (2015) Anodes for rechargeable lithium-sulfur batteries. Adv. Energy Mater. 5:1402273. https://doi.org/10.1002/aenm.201402273
29. Yan J, Liu X, Li B (2016) Capacity fade analysis of sulfur cathodes in lithium–sulfur batteries. Adv Sci 3:1600101. https://doi.org/10.1002/advs.201600101.
30. Choi YJ, Chung YD, Baek CY, Kim KW, Ahn HJ, Ahn HJ (2008) Effects of carbon coating on the electrochemical properties of sulfur cathode for lithium/sulfur cell. J Power Sources 184:548–552. https://www.sciencedirect.com/science/article/abs/pii/S0378775308003856
31. Ji X, Lee KT, Nazar LF (2009) A highly ordered nanostructured carbon - sulphur cathode for lithium - sulphur batteries. Nat Mater 8:500–506. https://www.nature.com/articles/nmat2460
32. Liu X, Huang JQ, Zhang Q, Mai L (2017) Nanostructured metal oxides and sulfides for lithium–sulfur batteries. Adv Mater 29:1601759. https://doi.org/10.1002/adma.201601759
33. He J, Manthiram A (2019) A review on the status and challenges of electrocatalysts in lithium-sulfur batteries. Energy Storage Mater 20:55–70. https://www.sciencedirect.com/science/article/abs/pii/S2405829719305100
34. Liang X, Hart C, Pang Q (2015) A highly efficient polysulfide mediator for lithium–sulfur batteries. Nat Commun 6:5682–5689. https://www.nature.com/articles/ncomms6682
35. Lin H, Zhang S, Zhang T, Ye H, Yao Q, Zheng GW, Lee JY (2018) Elucidating the catalytic activity of oxygen deficiency in the polysulfide conversion reactions of lithium–sulfur batteries. Adv Energy Mater 8:1801868. https://doi.org/10.1002/aenm.201801868
36. Guo Y, Zhang Y, Zhang Y (2018) Interwoven V_2O_5 nanowire/graphene nanoscroll hybrid assembled as efficient polysulfide-trapping-conversion interlayer for long-life lithium - sulfur batteries. J Mater Chem A 6:19358–19370. https://pubs.rsc.org/en/content/articlelanding/2018/ta/c8ta06610h
37. Hao Z, Chen J, Lu X., Kang L, Tan C, Xu R, Yuan L, Brett DJL, Shearing PR, Wang FR, Huang Y (2022) Precisely visit the performance modulation of functionalized separator in Li-S batteries via consecutive multiscale analysis. Energy Storage Mater 49:85–92. https://www.sciencedirect.com/science/article/pii/S2405829722001908
38. Ma L, Chen R, Zhu G, Hu Y, Wang Y, Chen T, Liu J, Jin Z (2017) Cerium oxide nanocrystal embedded bimodal micromesoporous nitrogen-rich carbon nanospheres as effective sulfur host for lithium–sulfur batteries. ACS Nano 11:7274–7283. https://doi.org/10.1021/acsnano.7b03227
39. Hu N, Lv X, Dai Y, Fan L, Xiong D, Li X (2018) SnO_2/reduced graphene oxide interlayer mitigating the shuttle effect of Li–S batteries. ACS Appl Mater Interfaces 10:18665–18674. https://doi.org/10.1021/acsami.8b03255
40. Zhou Y, Zhou C, Li, Q, Yan C, Han B, Xia K, Gao Q, Wu J (2015) Enabling prominent high-rate and cycle performances in one lithium–sulfur battery: designing perm selective gateways for Li^+ transportation in Holey-CNT/S cathodes. Adv Mater 27:3774–3781. https://doi.org/10.1002/adma.201501082
41. Ma XZ, Jin B, Wang HY, Hou JZ, Zhong XB, Wang HH, Xin PM (2015) S - TiO_2 composite cathode materials for lithium/sulfur batteries. J Electroanalytical Chem 736:127–131. https://www.sciencedirect.com/science/article/abs/pii/S1572665714004925
42. Zheng C, Niu S, Lv W (2017) Propelling polysulfides transformation for high-rate and long-life lithium–sulfur batteries. Nano Energy 33:306–312. https://www.sciencedirect.com/science/article/abs/pii/S2211285517300472?via%3Dihub
43. Pang Q, Kundu D, Cuisinier M, Nazar LF (2014) Surface-enhanced redox chemistry of polysulphides on a metallic and polar host for lithium-sulphur batteries. Nat Commun 5:4759–4766. https://www.nature.com/articles/ncomms5759
44. Chhowalla M, Shin HS, Eda G, Li LJ, Loh KP, Zhang H (2013) The chemistry of two-dimensional layered transition metal dichalcogenide nanosheets. Nat Chem 5:263–275. https://www.nature.com/articles/nchem.1589
45. Liu D, Zhang C, Zhou G, Lv W, Ling G, Zhi L, Yan QH (2018) Catalytic effects in lithium–sulfur batteries: promoted sulfur transformation and reduced shuttle effect. Adv Sci 5:1700270–1700281. https://doi.org/10.1002/advs.201700270
46. Yuan Z, Peng HJ, Hou TZ, Huang JQ, Chen CM, Wang DW, Cheng XB, Wei F, Zhang Q (2016) Powering lithium–sulfur battery performance by propelling polysulfide redox at sulfiphilic hosts. Nano Lett 16:519–527. https://doi.org/10.1021/acs.nanolett.5b04166
47. Babu G, Masurkar N, Salem HA, Arava LMR (2017) Transition metal dichalcogenide atomic layers for lithium polysulfides electrocatalysis. J Am Chem Soc 139:171–178. https://doi.org/10.1021/jacs.6b08681
48. Cho J, Ryu S, Gong YJ, Pyo S, Yun H, Kim H, Lee J, Yoo J, Kim US (2022) Nitrogen-doped MoS_2 as a catalytic sulfur host for lithium-sulfur batteries. Chem Eng J 439(1):135568. https://www.sciencedirect.com/science/article/abs/pii/S1385894722010701
49. Zhong Y, Xia X, Shi F, Zhan J, Tu J, Fan HJ (2016) Transition metal carbides and nitrides in energy storage and conversion. Adv Sci 3:1500286. https://doi.org/10.1002/advs.201500286
50. Ham DJ, Lee JS (2009) Transition metal carbides and nitrides as electrode materials for low temperature fuel cells. Energies 2:873–899. https://www.mdpi.com/1996-1073/2/4/873
51. Zhou F, Li Z, Luo X, Wu T, Jiang B, Lu LL, Yao HB, Antonietti M, Yu SH (2018) Low cost metal carbide nanocrystals as binding and electrocatalytic sites for high performance Li - S batteries. Nano Lett 18(2):1035–1043. https://doi.org/10.1021/acs.nanolett.7b04505
52. Salem HA, Chitturi VR, Babu G, Santana JA, Gopalakrishnan D, Arava LMR (2016) Stabilizing polysulfide-shuttle in a Li - S battery using transition metal carbide nanostructures. RSC Adv 6:110301–110306. https://pubs.rsc.org/en/content/articlelanding/2016/ra/c6ra22434b
53. Peng HJ, Zhang G, Chen X, Zhang ZW, Xu WT, Huang JQ, Zhang QJ (2016) Enhanced electrochemical kinetics on conductive polar mediators for lithium–sulfur batteries. Angew Chem Int Ed 55:12990–12995. https://doi.org/10.1002/anie.201605676
54. Choi J, Jeong TG, Cho BW, Yung Y, Oh SH, Kim YT (2018) Tungsten carbide as a highly efficient catalyst for polysulfide fragmentations in Li - S batteries. J Phys Chem C 122(14):7664–7669. https://doi.org/10.1021/acs.jpcc.8b02096
55. Luo L, Chung SH, Yaghoobnejad AH, Manthiram A (2018) Long-life lithium-sulfur batteries with a bifunctional cathode substrate configured with boron carbide nanowires. Adv Mater 30:e1804149. https://doi.org/10.1002/adma.201804149
56. Liu R, Liu W, Bu Y, Yang W, Wang C, Priest C, Liu Z, Wang Y, Cheng J, Lin X, Feng X, Wu G, Ma Y, Huang W (2020) Conductive porous laminated vanadium nitride as carbon-free hosts for high-loading sulfur cathodes in lithium–sulfur batteries. ACS Nano 14(12):17308–17320. https://doi.org/10.1021/acsnano.0c07415
57. Li X, Xu C, Zhao K, Wang Y, Pan L (2016) Carbon nitride based mesoporous materials as cathode matrix for high performance lithium–sulfur batteries. RSC Adv 6:13572–13580. https://pubs.rsc.org/en/content/articlelanding/2016/ra/c5ra26877j
58. Cui Z, Zu C, Zhou W (2016) Mesoporous titanium nitride-enabled highly stable lithium-sulfur batteries. Adv Mater 28(32):6926–6931. https://doi.org/10.1002/adma.201601382
59. Zeng W, Cheng MMC, Ng KYS (2019) Cathode framework of nanostructured titanium nitride/graphene for advanced lithium–sulfur batteries. ChemElectroChem 6(10):2796–2804. https://doi.org/10.1002/celc.201900364

60. Wu H, Jiang H, Yang Y (2020) Cobalt nitride nanoparticle coated hollow carbon spheres with nitrogen vacancies as an electrocatalyst for lithium–sulfur batteries. J Mater Chem A 8:14498–14505. https://pubs.rsc.org/en/content/articlelanding/2020/ta/d0ta05249c
61. Novoselov KS, Geim AK, Morozov SV (2004) Electric field effect in atomically thin carbon films. Science 306(5696):666–669. https://doi.org/10.1126/science.1102896
62. Guo S, Dong S (2011) Graphene nanosheet: synthesis, molecular engineering, thin film, hybrids, and energy and analytical applications. Chem Soc Rev 40(5):2644–2672. https://pubs.rsc.org/en/content/articlelanding/2011/cs/c0cs00079e
63. Naguib M, Gogotsi Y (2015) Synthesis of two-dimensional materials by selective extraction. Acc Chem Res 48(1):128–135. https://doi.org/10.1021/ar500346b
64. Naguib, M. Kurtoglu, V. Presser, Lu J, Niu J, Heon M, Hultman L, Gogotsi Y, Barsoum MW (2011) Two-dimensional nanocrystals produced by exfoliation of Ti_3AlC_2. Adv Mater 23(37):4248–4253. https://doi.org/10.1002/adma.201102306
65. Shein IR, Ivanovskii AL (2013) Graphene-like nanocarbides and nanonitrides of d metals (MXenes): synthesis, properties and simulation. Micro Nano Lett 8(2):59–62. https://doi.org/10.1049/mnl.2012.0797
66. Saeed MA, Shahzad A, Rasool K (2020) 2D MXene: a potential candidate for photovoltaic cells? A critical review. Adv Sci 10:2104743–2104765. https://doi.org/10.1002/advs.202104743
67. Chen X, Shi Z, Tian Y (2021) Two-dimensional Ti3C2 MXene-based nanostructures for emerging optoelectronic applications. Mater Horiz 8:2929–2963. https://pubs.rsc.org/en/content/articlelanding/2021/mh/d1mh00986a
68. Wojciechowski T, Wojciechowska AR, Matyszczak G (2019) Ti_2C MXene modified with ceramic oxide and noble metal nanoparticles: synthesis, morphostructural properties, and high photocatalytic activity. Inorg Chem 58(11):7602–7614. https://doi.org/10.1021/acs.inorgchem.9b01015
69. Gao L, Chen H, Kuklin AV (2022) Optical properties of few-layer Ti_3CN MXene: from experimental observations to theoretical calculations. ACS Nano 16(2):3059–3069. https://doi.org/10.1021/acsnano.1c10577
70. Naguib M, Mashtalir O, Carle J, Presser V, Lu J, Hultman L, Gogotsi Y, Barsoum MW (2012) Two-dimensional transition metal carbides. ACS Nano 6(2):1322–1331. https://doi.org/10.1021/nn204153h
71. Kurtoglu M, Naguib M, Gogotsi Y, Barsoum MW (2012) First principles study of two-dimensional early transition metal carbides. MRS Commun 2(4):133 -137. https://doi.org/10.1557/mrc.2012.25
72. Come J, Naguib M, Rozier P, Barsoum MW, Gogotsi Y, Taberna PL, Morcrette M, Simon P (2012) A non-aqueous asymmetric cell with a Ti_2C-based two-dimensional negative electrode. J Electrochem Soc 159(8):A1368. https://doi.org/10.1149/2.003208jes/pdf
73. Hu J, Xu B, Ouyang C, Yang SA, Yao Y (2014) Investigations on V_2C and V_2CX_2 (X = F, OH) monolayer as a promising anode material for li ion batteries from first principles calculations. J Phys Chem C 118(42):24274–24281. https://doi.org/10.1021/jp507336x
74. Liang X, Garsuch A, Nazar LF (2015) Sulfur cathodes based on conductive MXene nanosheets for high-performance lithium–sulfur batteries. Angew Chem Int Ed 54(13):3907–3911. https://doi.org/10.1002/anie.201410174
75. Rao D, Zhang L, Wang Y, Meng Z, Qian X, Liu J, Shen X, Qiao G, Lu R (2017) Mechanism on the improved performance of lithium sulfur batteries with MXene-based additives. J Phys Chem C 121:11047–11054. https://doi.org/10.1021/acs.jpcc.7b00492
76. Zhao Y, Zhao J (2017) Functional group-dependent anchoring effect of titanium carbide-based MXenes for lithium - sulfur batteries: a computational study. Appl Surf Sci 412:591–598. https://www.sciencedirect.com/science/article/abs/pii/S0169433217310103?via%3Dihub
77. Sim ES, Chung YC (2018) Non-uniformly functionalized titanium carbide-based MXenes as an anchoring material for Li-S batteries: a first-principles calculation. Appl Surf Sci 435:210–215. https://www.sciencedirect.com/science/article/abs/pii/S0169433217333731
78. Liu X, Shao X, Li F, Zhao M (2018) Anchoring effects of S-terminated Ti_2C MXene for lithium - sulfur batteries: a first-principles study. Appl Surf Sci 455:522–526. https://www.sciencedirect.com/science/article/abs/pii/S0169433218315277?via%3Dihub
79. Lin H, Yang DD, Lou N, Zhu SG, Li HZ (2019) Functionalized titanium nitride-based MXenes as promising host materials for lithium–sulfur batteries: a first principles study. Ceram Int 45:1588–1594. https://www.sciencedirect.com/science/article/pii/S0272884218328281?via%3Dihub
80. Li N, Meng Q, Zhu X, Li Z, Ma J, Huang C, Song J, Fan J (2019) Lattice constant-dependent anchoring effect of MXenes for lithium-sulfur (Li–S) batteries: a DFT study. Nanoscale 11:8485–8493. https://pubs.rsc.org/en/content/articlelanding/2019/nr/c9nr01220f
81. Liu Y, Wei H, Zhai X, Wang F, Ren X, Xiong Y, Akiyoshi O, Pan K, Ren F, Wei S (2021) Graphene-based interlayer for high-performance lithium–sulfur batteries: a review. Mater Des 211:110171–110202. https://www.sciencedirect.com/science/article/pii/S0264127521007267
82. Sang M, Shin J, Kim K, Yu KJ (2019) Electronic and thermal properties of graphene and recent advances in graphene based electronics applications. Nanomaterials 9:374–407. https://www.ncbi.nlm.nih.gov/pmc/articles/PMC6474003/#:~:text=Additionally%2C%20graphene%20is%20highly%20thermally,current%20to%20heat%20%5B18%5D.
83. Rizzi L, Zienert A, Shuster J, Köhne M, Shultz SE (2018) Electrical conductivity modeling of graphene-based conductor materials. ACS Appl. Mater. Interfaces 10(49):43088–43094. https://doi.org/10.1021/acsami.8b16361
84. Doñoro A, Mauricio AM, Etacheri V (2021) High-performance lithium sulfur batteries based on multidimensional graphene-CNT-nanosulfur hybrid cathodes. Batteries 7:26–42. https://www.mdpi.com/2313-0105/7/2/26
85. Zhang C, Ren L, Wang X, Liu T (2010) Graphene oxide -assisted dispersion of pristine multiwalled carbon nanotubes in aqueous media. J Phys Chem C 114:11435–11440. https://doi.org/10.1021/jp103745g
86. Wang H, Yang Y, Liang Y, Robinson JT, Li Y, Jackson A, Cui Y, Dai H (2011) Graphene-wrapped sulfur particles as a rechargeable lithium–sulfur battery cathode material with high capacity and cycling stability. Nano Lett 11(7):2644–2647. https://doi.org/10.1021/nl200658a
87. Wang X, Sun G, Routh P, Kim DH, Huang W, Chen P (2014) Heteroatom-doped graphene materials: syntheses, properties and applications. Chem Soc Rev 43:7067–7098. https://pubs.rsc.org/en/content/articlelanding/2014/cs/c4cs00141a
88. Agrawal K, Kishore N (2021) Computational study on adsorption characteristics of phenol and guaiacol over single and multiple nitrogen-doped graphene. Chem Select 6(30):7682–7690. https://doi.org/10.1002/slct.202102060
89. Jia Y, Zhao YS, Yang XX, Ren MX, Wang YQ, Lei BY, Zhao DL (2021) Sulfur encapsulated in nitrogen-doped graphene aerogel as a cathode material for high performance lithium-sulfur batteries. Int J Hydro Energy 46(10):7642–7652. https://www.sciencedirect.com/science/article/abs/pii/S0360319920344499?via%3Dihub
90. Wu P, Hu HY, Xie N, Wang C, Wu Fan, Pan M, Li HF, Wang XD, Zeng Z, Deng S, Dai GP (2019) A N-doped graphene–cobalt nickel sulfide aerogel as a sulfur host for lithium–sulfur batteries. RSC Adv 9:32247–32257. https://pubs.rsc.org/en/content/articlelanding/2019/ra/c9ra05202j
91. Thirumal V, Pandurangan A, Jayavel R, Ilangovan R (2016) Synthesis and characterization of boron doped graphene nanosheets for

supercapacitor applications. Synth Met 220:524–532. https://www.sciencedirect.com/science/article/abs/pii/S0379677916302351
92. Xie Y, Meng Z, Cai T, Han WQ (2015) Effect of boron-doping on the graphene aerogel used as cathode for the lithium–sulfur battery. ACS Appl Mater Interfaces 7(45):25202–25210. https://doi.org/10.1021/acsami.5b08129
93. Shi P, Wang Y, Liang X, Sun Y, Cheng S, Chen C, Xiang H (2018) Simultaneously exfoliated boron-doped graphene sheets to encapsulate sulfur for applications in lithium–sulfur batteries. ACS Sustainable Chem Eng 6(8):9661–9670. https://doi.org/10.1021/acssuschemeng.8b00378
94. Trindade T, O'Brien P, Pickett NL (2001) Nanocrystalline semiconductors: synthesis, properties, and perspectives. Chem Mater 13:3843–3858. https://doi.org/10.1021/cm000843p
95. Alivisatos AP (1996) Perspectives on the physical chemistry of semiconductor nanocrystals. J Phys Chem 100:13226–13239. https://doi.org/10.1021/jp9535506
96. Baker SN, Baker GA (2010) Luminescent carbon nanodots: emergent nanolights. Angew Chem Int Ed 49:6726–6744. https://doi.org/10.1002/anie.200906623
97. Fowley C, Nomikou N, McHale AP, McCaughan B, Callan JF (2013) Extending the tissue penetration capability of conventional photosensitisers: a carbon quantum dot - protoporphyrin IX conjugate for use in two-photon excited photodynamic therapy. Chem Commun 49:8934–8936. https://pubs.rsc.org/en/content/articlelanding/2013/cc/c3cc45181j#!
98. Zhao Z, Xie Y (2017) Enhanced electrochemical performance of carbon quantum dots-polyaniline hybrid. J Power Sources 337:54–64. https://www.sciencedirect.com/science/article/abs/pii/S0378775316315191?via%3Dihub
99. Liu WW, Feng YQ, Yan XB, Chen JT, Xue QJ (2013) Superior micro supercapacitors based on graphene quantum dots. Adv Funct Mater 23:4111–4122. https://doi.org/10.1002/adfm.201203771
100. Li J, Yun X, Hu Z, Xi L, Li N, Tang H, Lu P, Zhu Y (2019) Three-dimensional nitrogen and phosphorus co-doped carbon quantum dots/reduced graphene oxide composite aerogels with a hierarchical porous structure as superior electrode materials for supercapacitors. J Mater Chem A 7:26311–26325. https://pubs.rsc.org/en/content/articlelanding/2019/ta/c9ta08151h
101. Cai D, Wang L, Li L, Zhang Y, Li J, Chen D, Tu H, Han W (2019) Self-assembled CdS quantum dots in carbon nanotubes: induced polysulfide trapping and redox kinetics enhancement for improved lithium–sulfur battery performance. J Mater Chem A 7:806–815. https://pubs.rsc.org/en/content/articlelanding/2019/ta/c8ta09906e
102. Jian Z, Zhang S, Guan X, Li J, Li H, Wang W, Xing Y, Xu H (2020) ZnO quantum dot-modified rGO with enhanced electrochemical performance for lithium–sulfur batteries. RSC Adv 10:32966–32675. https://pubs.rsc.org/en/content/articlelanding/2020/ra/d0ra04986g
103. Zhao C, Zhou Y, Shi T, Guo D, Yin H, Song C, Qin L, Wang Z, Shao H, Yu K (2021) Employing synergetic effect of ZnSe quantum dots and layered $Ni(OH)_2$ to boost the performance of lithium–sulfur cathodes. Nanotechnology. 32 (50): 505406. https://iopscience.iop.org/article/https://doi.org/10.1088/1361-6528/ac2982
104. Artchuea T, Srikhaow A, Sriprachuabwong C, Tuantranont A, Tang IM, Pon-On W (2022) Copper Zinc Sulfide (CuZnS) Quantum dot-decorated(NiCo) S/conductive carbon matrix as the cathode for Li–S batteries. Nanomaterials 12:2403–2419. https://www.mdpi.com/2079-4991/12/14/2403
105. Xiao T, Yi F, Yang M, Liu W, Li M, Ren M, Zhang X, Zhou Z (2021) A composite of CoNiP quantum dot-decorated reduced graphene oxide as a sulfur host for Li–S batteries. J Mater Chem A 9:16692–16698. https://pubs.rsc.org/en/content/articlelanding/2021/TA/D1TA03608D
106. Park J, Moon J, Kim C, Kang JH, Lim E, Park J, Lee KJ, Yu SH, Seo JH, Lee J, Heo J, Tanaka N, Cho SP, Pyun J, Cabana J, Hong BH, Sung YE (2016) Graphene quantum dots: structural integrity and oxygen functional groups for high sulfur/sulfide utilization in lithium sulfur batteries. NPG Asia Mater 8:e272–281. https://www.nature.com/articles/am201661
107. Tong PH, Zhu L, Zang Y, Li J, He XP, James TD (2021) Metal–organic frameworks (MOFs) as host materials for the enhanced delivery of biomacromolecular therapeutics. Chem Commun 7:12098. https://pubs.rsc.org/en/content/articlelanding/2021/cc/d1cc05157a
108. Yaghi OM, Li H (1995) Hydrothermal synthesis of a metal-organic framework containing large rectangular channels. J Am Chem Soc 117(41):10401–10402. https://doi.org/10.1021/ja00146a033
109. Kitagawa S, Kaskel S, Xu Q (2022) Metal-organic frameworks: synthesis, structures, and applications. Small 3(5):2200072–2200073. https://doi.org/10.1002/sstr.202200072
110. Makiura R, Motoyama S, Umemura Y, Yamanaka H, Sakata O, Kitagawa H (2010) Surface nano-architecture of a metal - organic framework. Nat Mater 9:565–571. https://www.nature.com/articles/nmat2769
111. Xie, Z, Xu W, Cui X, Wang Y (2017) Recent progresses on metal-organic frameworks and their derived nanostructures for energy and environmental applications. Chemsuschem 10:1645–1663. https://doi.org/10.1002/cssc.201601855
112. Furukawa H, Cordova KE, O'Keeffe M, Yaghi OM (2013) The chemistry and applications of metal organic frameworks. Science 341:1230444. https://doi.org/10.1126/science.1230444
113. Li H, Eddaoudi M, O'Keeffe M, Yaghi OM (1999) Design and synthesis of an exceptionally stable and highly porous metal-organic framework. Nature 402:276–279. https://www.nature.com/articles/46248
114. Lawson HD, Walton SP, Chan C (2021) Metal organic frameworks for drug delivery: a design perspective. ACS Appl Mater Interfaces 13(6):7004–7020. https://doi.org/10.1021/acsami.1c01089
115. Li H, Wang K, Sun Y, Lollar CT, Li J, Zhou HC (2018) Recent advances in gas storage and separation using metal–organic frameworks. Mater Today 21(2):108–121. https://www.sciencedirect.com/science/article/pii/S1369702117302407
116. Bavykina A, Kolobov N, Khan IS, Bau JA, Ramirez A, Gascon J (2020) Metal–organic frameworks in heterogeneous catalysis: recent progress, new trends, and future perspectives. Chem Rev 120(16):8468–8535. https://doi.org/10.1021/acs.chemrev.9b00685
117. Russo V, Hmoudah M, Broccoli F, Lesce MR, Jung O, Serio MD (2020) Applications of metal organic frameworks in wastewater treatment: a review on adsorption and photodegradation. Front Chem Eng 2:581487–581499. https://doi.org/10.3389/fceng.2020.581487/full
118. Lin J, Reddy RCK, Zeng C, Lin X, Zeb A, Su CY (2021) Metal-organic frameworks and their derivatives as electrode materials for potassium ion batteries: A review. Coord. Chem. Rev. 446: 214118. https://www.sciencedirect.com/science/article/abs/pii/S0010854521003921
119. Morozan A, Jaouen F (2012) Metal organic frameworks for electrochemical applications. Energy Environ Sci 5:9269–9290. https://pubs.rsc.org/en/content/articlelanding/2012/ee/c2ee22989g
120. Zhou C, Li Z, Xu X, Mai L (2021) Metal-organic frameworks enable broad strategies for lithium-sulfur batteries. Natio Sci Rev 8:nwab055. https://academic.oup.com/nsr/article/8/12/nwab055/6226678
121. Bhargav A, He J, Gupta A, Manthiram A (2020) Lithium-sulfur batteries: attaining the critical metrics. Joule 4(2):285. https://www.sciencedirect.com/science/article/pii/S2542435120300015
122. Gao G, Feng W, Su W, Wang S, Chen L, Li M, Song C (2020) Preparation and modification of MIL-101(Cr) metal organic framework and its application in lithium-sulfur batteries. Int J Electrochem Sci 15:1426–1436. https://doi.org/10.20964/2020.02.26

123. Liu X, Wang S, Wang A, Chen J, Zeng Q, Chen P, Liu W, Li Z, Zhang L (2019) A new cathode material synthesized by a thiol-modified metal–organic framework (MOF) covalently connecting sulfur for superior long-cycling stability in lithium–sulfur batteries. J Mater Chem A 7:24515–24523. https://pubs.rsc.org/en/content/articlelanding/2019/ta/c9ta08043k
124. Chen D, Mukherjee S, Zhang C, Li Y., Xiao B, Singh CV (2022) Two-dimensional square metal organic framework as promising cathode material for lithium-sulfur battery with high theoretical energy density. J Colloid Interface Sci 613:435–446. https://www.sciencedirect.com/science/article/abs/pii/S0021979721021779?via%3Dihub
125. Feng Y, Zhang Y, Guixiang D, Zhang J, Qu X (2018) Experimental and first-principles study of a metal–organic framework with sulfur embedding cathode for enhanced performance lithium–sulfur battery. Sustainable Energy Fuels 2:1828–1836. https://pubs.rsc.org/en/content/articlehtml/2018/se/c8se00195b
126. Jiang H, Liu XC, Wu Y, Shu Y, Gong X, Ke FS, Deng H (2018) Metal-organic frameworks for high charge-discharge rate in lithium-sulfur battery. Angew Chem Int Ed Engl 57:3916–3921. https://doi.org/10.1002/anie.201712872
127. Wang S, Huang F, Zhang Z, Cai W, Jie Y, Wang S, Yan P, Jiao S, Cao R (2021) Conductive metal-organic frameworks promoting polysulfides transformation in lithium-sulfur batteries. J Energy Chem 63:336–343. https://www.sciencedirect.com/science/article/abs/pii/S2095495621004605
128. Chen K, Sun Z, Fang R, Shi Y, Cheng HM, Li F (2018) Metal–organic frameworks (MOFs)-derived nitrogen-doped porous carbon anchored on graphene with multifunctional effects for lithium–sulfur batteries. Adv Functional Mater 28(38):1707592. https://doi.org/10.1002/adfm.201707592
129. Wang C, Song H, Yu C, Ullah Z, Guan Z, Chu R, Zhang Y, Zhao L, Li Q, Liu L (2020) Iron single-atom catalyst anchored on nitrogen-rich MOF-derived carbon nanocage to accelerate polysulfide redox conversion for lithium sulfur batteries. J Mater Chem A 8:3421–3430
130. Itani H, Yokokawa K, Mori R (2022) Optimized electrolyte composition for lithium sulfur battery (PCT Application No. 2022–002252). Japanese Patent and Trademark Office
131. Yokokawa K, Itani H, Konishi K, Mori R (2022) Silicon coupling agent treatment of cathode material for lithium sulfur battery (Application No.2022–161750). Japanese Patent and Trademark Office
132. Liborio L, Mallia G (2009) Electronic structure of the Ti_4O_7 Magnéli Phase Phys Rev B 79:245133. https://doi.org/10.1103/PhysRevB.79.245133
133. Jaramillo TF, Jorgensen KP, Bonde J, Bielsen NJ, Horch, S, Chorkendorff I (2007) Identification of active edge sites for electrochemical H_2 evolution from MoS_2 nanocatalysts. Science 317:5834:100. https://doi.org/10.1126/science.1141483
134. Karunadasa HI, Montalvo E, Sun Y, Majda M, Long JR, Chang CJ (2012) A molecular MoS_2 edge site mimic for catalytic hydrogen generation. Science 335:6069:698. https://doi.org/10.1126/science.1215868
135. Wu D et al (2020) On the electronic structure and hydrogen evolution reaction activity of platinum group metal-based high-entropy-alloy nanoparticles. Chem Sci 11:12731. https://pubs.rsc.org/en/content/articlelanding/2020/sc/d0sc02351e
136. Yang Z et al (2016) Manipulating the d-band electronic structure of platinum-functionalized nanoporous gold bowls: synergistic intermetallic interactions enhance catalysis. Chem Mater 28(14):5080. https://doi.org/10.1021/acs.chemmater.6b01925
137. Liu J, Wei A, Pan G, Xiong Q, Chen F, Shen S, Xia X (2019) Atomic layer deposition-assisted construction of binder-free Ni@N-doped carbon nanospheres flms as advanced host for sulfur cathode. Nano-Micro Lett 11:64. https://doi.org/10.1007/s40820-019-0295-8
138. Meng Z, Li SJ, Ying HJ, Xu X, Zhu XL, Han WQ (2017) From silica sphere to hollow carbon nitride-based sphere: rational design of sulfur host with both chemisorption and physical confinement. Adv Mater Interfaces 4(11):1601195. https://doi.org/10.1002/admi.201601195
139. Acik M et al (2011) The role of oxygen during thermal reduction of graphene oxide studied by infrared absorption spectroscopy. J Phys Chem C 115:19761. https://doi.org/10.1021/jp2052618
140. Yeon JT, Jang JY, Han, JG, Cho J, Lee KT, Choi, NS (2012) Raman spectroscopy and X-ray diffraction studies of sulphur composite electrodes during discharge and charge. J Electrochem Soc 159:A1308. https://doi.org/10.1149/2.080208jes
141. Wang H et al (2011) Graphene–wrapped sulphur particles as a rechargeable lithium-sulphur battery cathode material with high capacity and cycling stability. Nano Lett 11:2644. https://doi.org/10.1021/nl200658a
142. Wang J et al (2020) Rational design of porous N-Ti_3C_2 MXene@CNT microspheres for high cycling stability in Li–S battery. Nano-Micro Lett 12:4. https://doi.org/10.1007/s40820-019-0341-6
143. Zong M et al (2021) A cost- and energy density-competitive lithium-sulfur battery. Energy Storage Mater 41:588. https://www.sciencedirect.com/science/article/pii/S2405829721003056
144. Soni R et al (2022) Lithium-sulfur battery diagnostics through distribution of relaxation times analysis. Energy Storage Mater 51:97. https://www.sciencedirect.com/science/article/pii/S2405829722003245
145. Barchasz C et al (2012) Lithium/sulfur cell discharge mechanism: an original approach for intermediate species identification. Anal Chem 84(9):3973. https://doi.org/10.1021/ac2032244
146. Fotouhi A, Auger DJ, O'Neill L, Cleaver T, Walus S (2022) Lithium-sulfur battery technology readiness and applications—a review. Energies 10:1937. https://www.mdpi.com/1996-1073/10/12/1937
147. Dörfler S et al (2020) Recent progress and emerging application areas for lithium–sulfur battery technology. Energy Technol 9(1):2000694. https://www.ncbi.nlm.nih.gov/pmc/articles/PMC7816250/
148. Yang L et al (2022) Atomic short-range order in a cation-deficient perovskite anode for fast-charging and long-life lithium-ion batteries. Adv Energy Mater 34(17):2200914. https://doi.org/10.1002/adma.202200914
149. Liang G et al (2020) Conductive $Li_{3.08}Cr_{0.02}Si_{0.09}V_{0.9}O_4$ anode material: novel "zero-strain" characteristic and superior electrochemical Li^+ storage. Adv Energy Mater 10(20):1904267. https://doi.org/10.1002/aenm.201904267
150. Yang L et al (2019) Conductive copper niobate: superior Li^+-storage capability and novel Li^+-transport mechanism. Adv Energy Mater 9(39):1902174. https://doi.org/10.1002/aenm.201902174
151. Yang L et al (2022) A new sodium calcium cyclotetravanadate framework: "zero-strain" during large-capacity lithium intercalation. Adv Funct Mater 32(1):2105026. https://doi.org/10.1002/adfm.202105026
152. Yang L et al (2021) Direct view on the origin of high Li^+ transfer impedance in all-solid-state battery. Adv Funct Mater 31(35):2103971. https://doi.org/10.1002/adfm.202103971
153. Xiong X et al (2022) A low strain A-site deficient perovskite lithium lanthanum niobate anode for superior Li+ storage. Adv Funct Mater 32(1):2106911. https://doi.org/10.1002/adfm.202106911
154. Liang G (2022) Interfacial space charge enhanced sodium storage in a zero-strain cerium niobite perovskite anode. Adv Funct Mater 32(43):2206129. https://doi.org/10.1002/adfm.202206129
155. Xiong X et al (2022) Cation-vacancy ordered superstructure enhanced cycling stability in tungsten bronze anode. Adv Energy Mater 12(36):2201967. https://doi.org/10.1002/aenm.202201967
156. Sevilla M, Rodríguez JC, Díez N, Fuertes AB (2020) Straightforward synthesis of Sulfur/N,S-codoped carbon cathodes for

Lithium-Sulfur batteries. Sci Rep 10:4866. https://www.nature.com/articles/s41598-020-61583-1
157. Zhang K et al (2020) Dual taming of polysufides by phosphorus-doped carbon for improving electrochemical performances of lithium–sulfur battery. Electrochimica Acta 354:136648. https://www.sciencedirect.com/science/article/abs/pii/S0013468620310410
158. Huang J, Wang N, Wang J, Huang N, Bayati M, Liu TX (2021) J Electroanal Chem 894(1):115362. https://www.sciencedirect.com/science/article/abs/pii/S157266572100388X
159. Zheng M et al (2019) Carbon nanotube-based materials for lithium–sulfur batteries. J Mater Chem A 2019(7):17204. https://pubs.rsc.org/en/content/articlelanding/2019/ta/c9ta05347f
160. Guo J, Xu Y, Wang C (2011) Sulfur-impregnated disordered carbon nanotubes cathode for lithium–sulfur batteries. Nano Lett 11(10):4288. https://doi.org/10.1021/nl202297p
161. Tian J, Xing F, Gao Q (2021) Graphene-based nanomaterials as the cathode for lithium-sulfur batteries. Molecules 26(9):2507. https://www.ncbi.nlm.nih.gov/pmc/articles/PMC8123287/